doi:10.1093/brain/aww027 BRAIN 2016: 139; 1551–1567 | 1551

BRAIN
A JOURNAL OF NEUROLOGY

Tau PET patterns mirror clinical and neuroanatomical variability in Alzheimer's disease

Rik Ossenkoppele,[1,2,3,*] Daniel R. Schonhaut,[1,2,*] Michael Schöll,[2,4] Samuel N. Lockhart,[2] Nagehan Ayakta,[1,2] Suzanne L. Baker,[5] James P. O'Neil,[5] Mustafa Janabi,[5] Andreas Lazaris,[1] Averill Cantwell,[1] Jacob Vogel,[2] Miguel Santos,[1] Zachary A. Miller,[1] Brianne M. Bettcher,[1,6] Keith A. Vossel,[1] Joel H. Kramer,[1] Maria L. Gorno-Tempini,[1] Bruce L. Miller,[1] William J. Jagust[2,5] and Gil D. Rabinovici[1,2]

[*]These authors contributed equally to this work.

See Sarazin *et al.* (doi:10.1093/brain/aww041) for a scientific commentary on this article.

The advent of the positron emission tomography tracer ^{18}F-AV1451 provides the unique opportunity to visualize the regional distribution of tau pathology in the living human brain. In this study, we tested the hypothesis that tau pathology is closely linked to symptomatology and patterns of glucose hypometabolism in Alzheimer's disease, in contrast to the more diffuse distribution of amyloid-β pathology. We included 20 patients meeting criteria for probable Alzheimer's disease dementia or mild cognitive impairment due to Alzheimer's disease, presenting with a variety of clinical phenotypes, and 15 amyloid-β-negative cognitively normal individuals, who underwent ^{18}F-AV1451 (tau), ^{11}C-PiB (amyloid-β) and ^{18}F-FDG (glucose metabolism) positron emission tomography, apolipoprotein E (*APOE*) genotyping and neuropsychological testing. Voxel-wise contrasts against controls (at $P < 0.05$ family-wise error corrected) showed that ^{18}F-AV1451 and ^{18}F-FDG patterns in patients with posterior cortical atrophy ('visual variant of Alzheimer's disease', $n = 7$) specifically targeted the clinically affected posterior brain regions, while ^{11}C-PiB bound diffusely throughout the neocortex. Patients with an amnestic-predominant presentation ($n = 5$) showed highest ^{18}F-AV1451 retention in medial temporal and lateral temporoparietal regions. Patients with logopenic variant primary progressive aphasia ('language variant of Alzheimer's disease', $n = 5$) demonstrated asymmetric left greater than right hemisphere ^{18}F-AV1451 uptake in three of five patients. Across 30 FreeSurfer-defined regions of interest in 16 Alzheimer's disease patients with all three positron emission tomography scans available, there was a strong negative association between ^{18}F-AV1451 and ^{18}F-FDG uptake (Pearson's $r = -0.49 \pm 0.07$, $P < 0.001$) and less pronounced positive associations between ^{11}C-PiB and ^{18}F-FDG (Pearson's $r = 0.16 \pm 0.09$, $P < 0.001$) and ^{18}F-AV1451 and ^{11}C-PiB (Pearson's $r = 0.18 \pm 0.09$, $P < 0.001$). Voxel-wise linear regressions thresholded at $P < 0.05$ (uncorrected) showed that, across all patients, younger age was associated with greater ^{18}F-AV1451 uptake in wide regions of the neocortex, while older age was associated with increased ^{18}F-AV1451 in the medial temporal lobe. *APOE* ε4 carriers showed greater temporal and parietal ^{18}F-AV1451 uptake than non-carriers. Finally, worse performance on domain-specific neuropsychological tests was associated with greater ^{18}F-AV1451 uptake in key regions implicated in memory (medial temporal lobes), visuospatial function (occipital, right temporoparietal cortex) and language (left > right temporoparietal cortex). In conclusion, tau imaging—contrary to amyloid-β imaging—shows a strong regional association with clinical and anatomical heterogeneity in Alzheimer's disease. Although preliminary, these results are consistent with and expand upon findings from post-mortem, animal and cerebrospinal fluid studies, and suggest that the pathological aggregation of tau is closely linked to patterns of neurodegeneration and clinical manifestations of Alzheimer's disease.

Received October 23, 2015. Revised December 21, 2015. Accepted January 11, 2016. Advance Access publication March 8, 2016

1 Memory and Aging Center, University of California San Francisco, San Francisco, CA, USA
2 Helen Wills Neuroscience Institute, University of California Berkeley, Berkeley, CA, USA
3 Department of Neurology and Alzheimer Center, Neuroscience Campus Amsterdam, VU University Medical Center, Amsterdam, The Netherlands
4 MedTech West and the Department of Clinical Neuroscience and Rehabilitation, University of Gothenburg, Sweden
5 Life Sciences Division, Lawrence Berkeley National Laboratory, Berkeley, CA, USA
6 Rocky Mountain Alzheimer's Disease Center, Departments of Neurosurgery and Neurology, University of Colorado Denver Anschutz Medical Campus, Aurora, CO, USA

Correspondence to: Rik Ossenkoppele,
Memory and Aging Center,
University of California San Francisco,
675 Nelson Rising Lane,
Suite 190, San Francisco,
CA94158, USA
E-mail: r.ossenkoppele@vumc.nl

Keywords: Alzheimer's disease; tau; AV1451 PET; cognition; APOE

Abbreviations: AI = asymmetry index; DVR = distribution volume ratio; MMSE = Mini-Mental State Examination; PCA = posterior cortical atrophy; PiB = Pittsburgh compound B; PPA = primary progressive aphasia; SUVR = standardized uptake value ratio

Introduction

The ability to detect fibrillar amyloid-β plaque depositions using ^{11}C-Pittsburgh compound B (PiB; Klunk *et al.*, 2004) or fluorinated amyloid PET tracers (Vandenberghe *et al.*, 2010; Barthel *et al.*, 2011; Clark *et al.*, 2011) has had a major impact on the field of Alzheimer's disease. Among many other applications, amyloid-β imaging has been incorporated into diagnostic criteria for various stages of the disease (Albert *et al.*, 2011; McKhann *et al.*, 2011; Sperling *et al.*, 2011; Dubois *et al.*, 2014), has substantial impact on clinical decision-making (Ossenkoppele *et al.*, 2013*a*; Sanchez-Juan *et al.*, 2014) and patient management plans (Schipke *et al.*, 2012; Grundman *et al.*, 2013), and has shown potential as a surrogate outcome measure in clinical trials tailored to reduce cerebral amyloid-β plaque burden (Salloway *et al.*, 2014; Liu *et al.*, 2015). A yet unresolved issue after a decade of amyloid-β imaging research, however, is the disconnection between the diffuse distribution of amyloid-β pathology throughout the neocortex (Rabinovici *et al.*, 2010; Wolk *et al.*, 2012; Lehmann *et al.*, 2013; Jung *et al.*, 2015) and the selective patterns of brain atrophy and glucose hypometabolism that strongly correlate with clinical symptoms (Rabinovici *et al.*, 2010; Ridgway *et al.*, 2012; Lehmann *et al.*, 2013; Madhavan *et al.*, 2013). Thus, although amyloid-β deposition may be a prerequisite to developing Alzheimer's disease dementia, at some point during the disease course additional factors are likely involved in determining regional neurodegeneration and symptomatology.

Tau, a microtubule-associated protein that aggregates into intracellular neurofibrillary tangles in Alzheimer's disease (Weingarten *et al.*, 1975; Braak and Braak, 1991), has often been suggested as a facilitator of the downstream effects of amyloid-β (Desikan *et al.*, 2012; Jack and Holtzman, 2013). Tau pathology has a devastating effect on synaptic function (Gomez-Isla *et al.*, 1997; Beharry *et al.*, 2014; Spires-Jones and Hyman, 2014) and relates more strongly to cognitive functions during life than does amyloid-β (Arriagada *et al.*, 1992; Nelson *et al.*, 2012; van Rossum *et al.*, 2012; Rolstad *et al.*, 2013). However, current knowledge about relationships between tau pathology and other disease measures is mainly derived from animal, neuropathological and CSF studies. The recent advent of a PET tracer (i.e. ^{18}F-AV1451, formerly called ^{18}F-T807), which shows high affinity and selectivity for paired helical filament tau pathology *in vitro* (Chien *et al.*, 2013; Xia *et al.*, 2013; Marquie *et al.*, 2015), now allows *in vivo* assessment of regional tau load.

Mapping the distribution of tau pathology may further our understanding of disease mechanisms in distinct clinical variants of Alzheimer's disease. These clinical variants include posterior cortical atrophy (PCA, 'visual variant of Alzheimer's disease'; Crutch *et al.*, 2012), logopenic variant primary progressive aphasia (logopenic variant PPA, 'language variant of Alzheimer's disease'; Gorno-Tempini *et al.*, 2011), corticobasal syndrome (Alzheimer's disease pathology is the causative pathology in up to 25% of cases; Dickson *et al.*, 2002; Lee *et al.*, 2011), and memory-predominant and behavioural/dysexecutive variants of Alzheimer's disease (Ossenkoppele *et al.*, 2015*c*). Age at onset has also been associated with clinical and anatomical variability; while patients with late-onset Alzheimer's disease ($\geq$65 years of age) typically present with amnestic symptoms and medial temporal lobe neurodegeneration, patients with early-onset ($<$65 years) tend to exhibit greater non-amnestic deficits and neocortical-predominant atrophy (Rabinovici *et al.*, 2010; Mendez *et al.*, 2012;

Ossenkoppele *et al.*, 2012; Smits *et al.*, 2012; Moller *et al.*, 2013; Cavedo *et al.*, 2014). Furthermore, patients with Alzheimer's disease who carry the apolipoprotein E (*APOE*) ε4 allele have shown greater medial temporal lobe vulnerability (Pievani *et al.*, 2009; van der Flier *et al.*, 2011; Ossenkoppele *et al.*, 2013*b*; Lehmann *et al.*, 2014) and post-mortem tau pathology (Beffert and Poirier, 1996; Tiraboschi *et al.*, 2004) compared to non-carriers.

In a recent case study of a patient with PCA, ^{18}F-AV1451 was found to be more closely linked to hypometabolism and cognitive deficits than was amyloid-β (Ossenkoppele *et al.*, 2015*d*). Here we extend these findings in a larger sample and across multiple phenotypes, studying associations between tau pathology and factors that underlie heterogeneity in the manifestation of Alzheimer's disease. We hypothesized that: (i) ^{18}F-AV1451 would show distinct patterns in clinical variants of Alzheimer's disease, in early-onset versus late-onset Alzheimer's disease and in *APOE* ε4 carriers versus non-carriers; and (ii) the amount and distribution of ^{18}F-AV1451 retention would correlate with neuropsychological performance.

Materials and methods

Participants

Twenty patients were recruited from the University of California San Francisco (UCSF) Alzheimer's Disease Research Center. This represents a consecutive series of recruited research participants who met clinical criteria for probable Alzheimer's disease dementia (McKhann *et al.*, 2011) or mild cognitive impairment (Albert *et al.*, 2011) due to Alzheimer's disease, who underwent ^{18}F-AV1451 PET scans between June 2014 and June 2015. All patients underwent a medical history and physical examination, a structured caregiver interview, brain MRI and neuropsychological testing. Seven patients met specific diagnostic criteria for PCA (Mendez *et al.*, 2002), five for logopenic variant PPA (Gorno-Tempini *et al.*, 2011), and one for corticobasal syndrome (Armstrong, 2014). Based on chart reviews and evaluation of the neuropsychological reports, the remaining patients were classified as amnestic ($n = 5$) and behavioural/dysexecutive variant Alzheimer's disease ($n = 1$; Ossenkoppele *et al.*, 2015*c*). One patient (59-year-old male) presented with a history of focal cortical deficits (i.e. agnosia, aphasia, apraxia) with relative preservation of memory function. This patient did not meet formal criteria for any of the Alzheimer's disease variants, and will be referred to as 'non-amnestic Alzheimer's disease'. Nineteen (95%) patients had a visually positive PiB-PET scan as assessed according to previously published procedures (Rabinovici *et al.*, 2010). Amyloid-β status was unknown for one patient with a clinical diagnosis of logopenic variant PPA. Exclusion criteria were: (i) meeting core clinical criteria for another dementia; (ii) clinically significant cerebrovascular disease; (iii) major systemic disease; (iv) history of a neurological disorder causing dementia; or (v) recent history of substance abuse.

In addition, 15 cognitively normal controls were recruited through the Berkeley Aging Cohort. The eligibility criteria for controls include a minimum age of 60, preventing a more accurate age matching of controls to the relatively young patients in the present study. Further eligibility criteria included normal performance on cognitive tests, absence of neurological or psychiatric illness that potentially affects brain structure and function (including white matter abnormalities) and lack of major medical illnesses and medications that affect cognition. To enhance contrasts between Alzheimer's disease and normal ageing, we excluded 12 additional control studies with ^{18}F-AV1451 and ^{11}C-PiB who met criteria for preclinical Alzheimer's disease (Sperling *et al.*, 2011) based on positive PiB-PET [distribution volume ratio (DVR) $\geqslant 1.08$; Mormino *et al.*, 2012]. Informed consent was obtained from all subjects or their assigned surrogate decision-makers, and UCSF, University of California Berkeley, and the Lawrence Berkeley National Laboratory (LBNL) institutional review boards for human research approved the study.

MRI

All patients and controls underwent MRI on a 3 T Siemens Tim Trio scanner or 1.5 T Magnetom Avanto scanner, respectively. Sequences included T_1-weighted magnetization prepared rapid gradient echo (MP-RAGE) for structure and fluid attenuation inversion recovery (FLAIR) to assess cerebrovascular disease [(Villeneuve *et al.*, 2014; Ossenkoppele *et al.*, 2015*a*), see specifications in Supplementary material]. MP-RAGE sequences were processed using FreeSurfer 5.1 (Fischl *et al.*, 2002) to define native-space reference regions and cortical regions of interest.

Positron emission tomography

PET scans were performed at LBNL on a Siemens Biograph 6 Truepoint PET/CT scanner in 3D acquisition mode, and on a ECAT EXACT HR scanner for a small subset of ^{11}C-PiB ($n = 3$) and ^{18}F-FDG ($n = 3$) PET scans in controls. A low-dose CT/transmission scan was performed for attenuation correction prior to all scans. ^{11}C-PiB and ^{18}F-FDG PET scans were performed as previously described (Lehmann *et al.*, 2013). ^{18}F-AV1451 was synthesized and radiolabelled at LBNL's Biomedical Isotope Facility. Approximately 10 mCi of ^{18}F-AV1451 was injected intravenously, and subjects participated in one of two acquisition schemes: 0–100-min post-injection full dynamic scans (4×15, 8×30, 9×60 s, and 2×3, 16×5 min frames) followed by 120–150 min (6×5 min frames: 13 controls, 15 patients), or 75–115 min (8×5 min frames: two control subjects, five patients). PET data were reconstructed using an ordered subset expectation maximization algorithm with weighted attenuation. Images were smoothed with a 4 mm Gaussian kernel with scatter correction and evaluated prior to analysis for patient motion and adequacy of statistical counts. All PET scans were acquired within an average of 68 ± 109 days (^{18}F-AV1451 to ^{18}F-FDG: 105 ± 122 days, ^{18}F-AV1451 to ^{11}C-PiB: 95 ± 121 days, ^{18}F-FDG to ^{11}C-PiB: 0 ± 2 days).

Image analyses

PET images were co-registered to the subjects' MP-RAGE using Statistical Parametric Mapping (SPM) version 8

(Wellcome Trust Centre for Neuroimaging, Institute of Neurology at University College London). Dynamic 90 min ^{11}C-PiB data were analysed using Logan graphical analysis with FreeSurfer-derived grey matter cerebellum as the reference region, yielding voxelwise DVR (Logan *et al.*, 1996). One patient did not undergo ^{11}C-PiB PET, and two patients had no ^{11}C-PiB dynamic data available (but were positive on visual read of semiquantitative parametric images), yielding a total of 17/20 patients with ^{11}C-PiB DVR data. ^{18}F-FDG PET images were summed, and standardized uptake value ratios (SUVR) were calculated for the 30–60-min post-injection interval using mean activity in the pons (manually edited from FreeSurfer-derived brainstem) as the reference region (Minoshima *et al.*, 1995). Sixteen patients had ^{18}F-FDG PET data available. Consistent with the initial report on human ^{18}F-AV1451/^{18}F-T807 PET (Chien *et al.*, 2013), SUVR images at t = 80–100 minutes post-injection were created by normalizing summed activity from the realigned frames to mean activity in cerebellar grey matter, an area relatively spared of neurofibrillary tangle pathology even in advanced Alzheimer's disease (Braak and Braak, 1991; Marquie *et al.*, 2015). $SUVR_{80–100}$ showed the highest correlation across all time intervals with non-displaceable binding potentials derived from analyses with simplified reference tissue model 2 (SRTM2) in 23 controls and 15 patients with Alzheimer's disease with dynamic data available (data not shown), and was therefore the interval of choice. We performed partial volume correction on all tracers using the Geometric Transfer Matrix approach (Rousset *et al.*, 1998) and report both corrected and uncorrected data for region of interest analyses.

APOE status

Genotyping of the *APOE* allele (rs429358 and rs7412) was performed using a TaqMan® Allelic Discrimination Assay on an ABI 7900HT Fast Real-Time PCR system (Applied Biosystems) according to a previously described methodology (Coppola *et al.*, 2012). *APOE* ε4 status was determined in 19/20 patients.

Neuropsychology

Within 1 year of the ^{18}F-AV1451 PET scan (mean interval: 112 ± 83 days), 18/20 patients underwent a neuropsychological test battery that covered four major cognitive domains (Kramer *et al.*, 2003; Lehmann *et al.*, 2013; Ossenkoppele *et al.*, 2015*a*): memory [immediate recall, delayed free recall, delayed cued recall and delayed recognition of the California Verbal Learning Test (9 items), and delayed recall of the Benson Figure], visuospatial or parietal function (copy of the Benson Figure, design fluency, calculations, face matching, and number location of the Visual Object and Space Perception battery), executive function [Modified Trail-making time and accuracy, Stroop interference (*n* correct and *n* errors), Digit Span backward, verbal fluency (D-words), and abstraction], and language [sentence repetition and comprehension, verbal agility, letter/word reading, picture vocabulary, category fluency (animals), and the Boston Naming Test]. Raw test scores were z-transformed using means and standard deviations (SD) of a group of 574 cognitively normal individuals [42.5% male, mean age: 66.1 ± 11.4, education: 17.2 ± 2.4, Mini-Mental State Examination (MMSE): 29.2 ± 1.1, all with a Clinical Dementia Rating (CDR) of 0 and a Geriatric Depression Scale (GDS) score ⩽ 5] recruited at UCSF. Subsequently, these z-scores were averaged across all neuropsychological tests within a domain, resulting in composite scores for each cognitive domain.

Statistics

Baseline demographic and clinical features

Differences in baseline characteristics between groups were assessed using ANOVA with *post hoc* Bonferroni tests for continuous variables and χ^2 and Kruskal-Wallis with *post hoc* Mann-Whitney U-tests for dichotomous or categorical data.

Voxelwise contrasts between patients and controls

For voxelwise statistical analyses in SPM8, parametric PET images were spatially normalized to Montreal Neurological Institute space, followed by smoothing using an 8 mm isotropic Gaussian kernel. Then, voxelwise contrasts were performed to examine differences in ^{18}F-AV1451, ^{11}C-PiB and ^{18}F-FDG PET uptake in patients with PCA against healthy controls. Similar contrasts were performed between patients with logopenic variant PPA and amnestic Alzheimer's disease against controls for ^{18}F-AV1451 only, as ^{11}C-PiB and ^{18}F-FDG were not available in all patients. The contrasts were thresholded at $P < 0.05$ family-wise error corrected, without adjustment for nuisance variables.

Region of interest analyses for ^{18}F-AV1451, ^{11}C-PiB and ^{18}F-FDG PET

Mean SUVR (^{18}F-AV1451 and ^{18}F-FDG) and DVR (^{11}C-PiB) values were extracted for FreeSurfer-defined frontal (superior and middle gyri and orbitofrontal cortex), lateral temporal (superior, middle and inferior gyri), lateral parietal (inferior, superior and suprmarginal gyri), medial parietal (posterior cingulate and precuneus), occipital (calcarine, cuneus and lateral occipital cortex), medial temporal (hippocampus, entorhinal cortex and parahippocampus), and basal ganglia (putamen, caudate and pallidum). These regions were selected as we aimed to assess the full spectrum of Braak stages (Braak and Braak, 1991) as well as 'off-target' tracer uptake in basal ganglia structures (Marquie *et al.*, 2015; Johnson *et al.*, 2016). We also calculated a hemispheric asymmetry index [AI, similar to Rabinovici *et al.* (2008) and Frings *et al.* (2015)] for each region of interest using the formula AI [%] = 200 × (R − L)/(R + L) for ^{18}F-AV1451 and ^{11}C-PiB, or AI [%] = −200 × (R − L)/(R + L) for ^{18}F-FDG. Thus, negative outcomes indicate more tau and amyloid-β, or more severe glucose hypometabolism in the left hemisphere, while positive values reflect right lateralized asymmetry. Differences in uptake values were assessed using ANOVA with *post hoc* Bonferroni tests.

Next, we performed Pearson correlations between the three PET tracers across 30 *a priori* selected left and right cortical [i.e. frontal, parietal, lateral temporal and occipital: based on Ossenkoppele *et al.* (2015*d*)] FreeSurfer regions of interest in native MRI space across 16 patients with Alzheimer's disease with all tracers available. To control for interdependency resulting from multiple measurements (i.e. regions of interest) per subject, we additionally performed mixed effects models

Table 1 Demographic and clinical characteristics according to diagnostic group

	Posterior cortical atrophy	Logopenic variant PPA	Amnestic Alzheimer's disease	Non-amnestic Alzheimer's disease	Behavioural/dysexecutive variant Alzheimer's disease	Corticobasal syndrome	Controls
n	7	5	5	1	1	1	15
Age	63 ± 10	65 ± 10	67 ± 8	59	59	60	79 ± 7[a]
Sex (male/female)	4/3	1/4	3/2	1/0	1/0	0/1	6/9
Education (years)	15 ± 1	18 ± 2	17 ± 3	24	16	16	17 ± 1
Handedness (R/L/A)	6/1/0	3/2/0	4/0/0 (1 NA)	1/0/0	0/0/1	1/0/0	14/0/1
PiB status (+/−)	7/0	4/0 (1 NA)	5/0	1/0	1/0	1/0	0/15
PiB global DVR	1.86 ± 0.13	1.84 ± 0.38	1.79 ± 0.43	1.86	1.94	1.64	1.05 ± 0.03
APOE ε4 (+/−)	4/3	2/5	3/5	0/1	0/1	–	2/12
CDR	0.9 ± 0.2	0.6 ± 0.2	0.7 ± 0.3	0.5	1	–	–
MMSE	23 ± 4	18 ± 8	20 ± 5	27	21	16	29 ± 1[a]
Memory z-score	−2.5 ± 1.3	−2.6 ± 1.5	−3.4 ± 1.0	−1.5	−2.5	–	–
Visuospatial z-score	−5.9 ± 2.9[b]	−1.9 ± 1.9	−2.0 ± 1.4	−0.8	−1.4	–	–
Executive z-score	−2.9 ± 2.0	−3.7 ± 2.5	−1.9 ± 1.9	−0.8	−2.4	–	–
Language z-score	−2.1 ± 0.9	−4.0 ± 1.6[c]	−1.7 ± 1.4	−0.3	−0.3	–	–

Differences in baseline characteristics between groups ($n > 1$) were assessed using ANOVA with *post hoc* Bonferroni tests for continuous variables and χ^2 and Kruskal-Wallis with *post hoc* Mann-Whitney U-tests for dichotomous or categorical data.
[a]Controls > patients, $P < 0.05$.
[b]Posterior cortical atrophy < Logopenic variant primary progressive aphasia and amnestic Alzheimer's disease, $P < 0.05$.
[c]Logopenic variant primary progressive aphasia < posterior cortical atrophy and amnestic Alzheimer's disease, $P < 0.05$.
A = ambidextrous; CDR = Clinical Dementia Rating; R = right; L = left; NA = not available.

(i.e. a single model for each tracer comparison) assuming random intercepts and fixed slopes, using the maximum likelihood method for parameter estimation and likelihood ratio tests to assess significance.

Relationships between ^{18}F-AV1451 with age, *APOE* and cognition

We conducted separate whole-brain voxelwise linear regressions between ^{18}F-AV1451 uptake and age, *APOE* ε4 allele status (carrier or non-carrier), MMSE, and composite scores on four different cognitive domains (memory, visuospatial, executive and language functions) across all patients with Alzheimer's disease. These analyses were thresholded at $P < 0.05$ uncorrected for multiple comparisons. In the model exploring effects of APOE ε4 allele status on voxelwise ^{18}F-AV1451 uptake, analyses were performed with and without adjusting for global amyloid-β burden (measured as mean ^{11}C-PiB retention in prefrontal, lateral temporal, parietal, and cingulate cortices; Ossenkoppele *et al.*, 2014). Other analyses were performed without adjustment for nuisance variables. Finally, we performed region of interest analyses to test associations between regional ^{18}F-AV1451 uptake patterns and age, memory, visuospatial performance and language ability. Rank correlations (Spearman's rho or Kendall's τ in case of ties) were calculated between age and the ratio of hippocampal to cortical ^{18}F-AV1451, memory score and hippocampal ^{18}F-AV1451, visuospatial score and occipital ^{18}F-AV1451, and language and left temporoparietal ^{18}F-AV1451. We examined the regional specificity of these correlations by relating composite cognitive scores to ^{18}F-AV1451 uptake in control regions of interest: memory score and cortical (i.e. weighted average of frontal, temporal, parietal and occipital cortex) ^{18}F-AV1451, visuospatial score and cortical ^{18}F-AV1451, and language score and right temporoparietal/whole cortex ^{18}F-AV1451. A schematic overview and visual representations of the FreeSurfer-defined regions of interest are provided in Supplementary Table 1 and Supplementary Fig. 1, respectively.

Results

Patients

Demographic and clinical characteristics are presented in Table 1. The Alzheimer's disease patients were on average relatively young (64 ± 8 years on average across phenotypes) and in a mild stage of the disease (mean MMSE: 21 ± 6). As expected, patients with PCA showed more severe impairment on visuospatial tasks than patients with logopenic variant PPA or an amnestic-predominant presentation ($P < 0.05$), while patients with logopenic variant PPA performed worse on language tests than the other two groups ($P < 0.05$).

Control subjects

The healthy controls were substantially older (79 ± 7 years) than the Alzheimer's disease patients and 14% carried an *APOE* ε4 allele. In line with a recent study (Johnson *et al.*, 2016), visual inspection and regional quantification of ^{18}F-AV1451 images (Table 2 and Supplementary Fig. 2) showed some degree of uptake in medial temporal lobes (i.e. entorhinal cortex, parahippocampal gyrus and hippocampus) in all normal subjects. According to the staging proposed by Braak and Braak (1991), this pattern extended into fusiform gyrus and inferior temporal cortex in several

Table 2 ^{18}F-AV1451, ^{18}F-FDG and ^{11}C-PiB retention values and asymmetry indices in regions of interest

	PCA		Logopenic variant PPA		Amnestic Alzheimer's disease		Controls	
	SUVR	AI (%)	SUVR	AI (%)	SUVR	AI (%)	SUVR	AI (%)
^{18}F-AV1451								
Frontal	1.57 ± 0.33	8.8 ± 14.9	1.76 ± 0.59	−11.8 ± 18.5	1.55 ± 0.39	−2.5 ± 14.0	1.07 ± 0.06[d]	0.4 ± 1.4
Lateral temporal	2.09 ± 0.47	8.8 ± 10.6	2.43 ± 0.47	−4.2 ± 10.0	2.05 ± 0.28	−8.4 ± 17.1	1.11 ± 0.05[d]	−0.1 ± 2.1
Lateral parietal	2.42 ± 0.50	3.6 ± 12.3	2.28 ± 0.74	−13.5 ± 14.5	2.03 ± 0.47	−5.8 ± 20.0	1.08 ± 0.08[d]	−0.4 ± 2.8
Medial parietal	2.47 ± 0.55[a]	9.7 ± 13.3	2.11 ± 0.48	−12.4 ± 15.5	1.93 ± 0.45	−4.8 ± 18.6	1.12 ± 0.09[d]	1.2 ± 2.1
Occipital	2.16 ± 0.43[b]	11.3 ± 8.7	1.65 ± 0.17	−7.5 ± 10.8	1.42 ± 0.31	1.3 ± 17.9	1.06 ± 0.06[d]	1.3 ± 2.0
Medial temporal	1.43 ± 0.20	1.9 ± 5.5	1.41 ± 0.25	−1.9 ± 7.1	1.70 ± 0.33[c]	−4.9 ± 7.3	1.18 ± 0.06[d]	−0.5 ± 4.6
Basal ganglia	1.33 ± 0.14	3.0 ± 4.2	1.21 ± 0.23	−3.3 ± 7.3	1.44 ± 0.11	−3.4 ± 7.9	1.47 ± 0.15[e]	−1.3 ± 2.6
	n = 7		*n* = 5		*n* = 5		*n* = 15	
^{18}F-FDG								
Frontal	1.43 ± 0.06	3.0 ± 6.6	1.51 ± 0.03	−10.8 ± 6.2	1.40 ± 0.18	−6.6 ± 9.1	1.48 ± 0.08	−1.1 ± 2.2
Lateral temporal	1.13 ± 0.09[f]	11.3 ± 14.6	1.14 ± 0.20	−12.3 ± 0.8	1.18 ± 0.04	−9.0 ± 14.1	1.34 ± 0.12	0.3 ± 2.6[h]
Lateral parietal	1.07 ± 0.08[f]	16.3 ± 17.3	1.25 ± 0.15	−14.9 ± 1.5	1.32 ± 0.08	−6.4 ± 12.9	1.48 ± 0.14	0.2 ± 2.3[h]
Medial parietal	1.34 ± 0.06[f]	15.2 ± 13.4	1.35 ± 0.36	−18.6 ± 6.1	1.51 ± 0.14	−5.9 ± 10.0	1.65 ± 0.11	−3.0 ± 2.2[i]
Occipital	1.28 ± 0.23[g]	11.7 ± 17.4	1.72 ± 0.24	−6.5 ± 3.2	1.64 ± 0.10	−1.6 ± 6.2	1.54 ± 0.11	−2.0 ± 2.1[j]
Medial temporal	1.02 ± 0.09	5.8 ± 8.6	1.10 ± 0.03	−6.1 ± 4.3	1.03 ± 0.03	−7.5 ± 7.9	1.10 ± 0.06	−0.6 ± 2.9[j]
Basal ganglia	1.43 ± 0.04	1.7 ± 8.2	1.60 ± 0.17	−5.3 ± 2.5	1.46 ± 0.10	−5.0 ± 4.6	1.51 ± 0.13	0.1 ± 2.9
	n = 7		*n* = 2		*n* = 4		*n* = 13	
	DVR	AI (%)	DVR	AI (%)	DVR	AI (%)	DVR	AI (%)
^{11}C-PiB								
Frontal	1.84 ± 0.16	1.6 ± 4.7	1.91 ± 0.50	−3.1 ± 6.8	1.61 ± 0.29	4.9 ± 5.6	1.00 ± 0.04[k]	0.4 ± 1.3
Lateral temporal	1.65 ± 0.16	−1.9 ± 6.1	1.73 ± 0.39	−0.1 ± 2.5	1.51 ± 0.26	3.8 ± 3.4	0.99 ± 0.02[k]	−1.0 ± 3.0
Lateral parietal	1.73 ± 0.12	−3.1 ± 5.2	1.85 ± 0.26	1.9 ± 3.8	1.61 ± 0.31	2.12 ± 4.5	1.04 ± 0.03[k]	−0.9 ± 2.4
Medial parietal	1.97 ± 0.15	−1.4 ± 2.6	2.04 ± 0.25	0.6 ± 9.1	1.82 ± 0.33	−0.1 ± 0.6	1.10 ± 0.04[k]	1.7 ± 3.7
Occipital	1.50 ± 0.14	2.8 ± 5.6[l]	1.58 ± 0.23	−5.2 ± 2.2	1.31 ± 0.17	3.4 ± 3.5	1.04 ± 0.03[k]	1.0 ± 3.4
Medial temporal	1.14 ± 0.08	−1.9 ± 6.2	1.21 ± 0.12	2.8 ± 5.0	1.10 ± 0.08	7.5 ± 3.1	0.98 ± 0.05[k]	0.8 ± 3.0
Basal ganglia	1.68 ± 0.16	1.3 ± 4.3	1.70 ± 0.31	−0.7 ± 2.7	1.60 ± 0.18	1.6 ± 4.5	1.23 ± 0.06[k]	−0.8 ± 1.8
	n = 7		*n* = 3		*n* = 4		*n* = 15	

Data are presented as group means ± SD; see Fig. 3 for individual data. AI for ^{18}F-AV1451 and ^{11}C-PiB were calculated using AI [%] = 200 × (R − L) / (R + L), and AI [%] = -200 × (R − L) / (R + L) for ^{18}F-FDG. Negative values indicate greater AV1451 and PiB, and reduced FDG uptake in the left compared to the right hemisphere. Differences between groups for SUVR were assessed using ANOVA with *post hoc* Bonferroni tests at $P < 0.05$: [a]PCA > amnestic Alzheimer's disease; [b]PCA > logopenic variant PPA and amnestic Alzheimer's disease; [c]Amnestic Alzheimer's disease > PCA and logopenic variant PPA; [d]Controls < PCA, logopenic variant PPA and amnestic Alzheimer's disease; [e]Controls > logopenic variant PPA; [f]PCA < amnestic Alzheimer's disease; [g]PCA < logopenic variant PPA and amnestic Alzheimer's disease; [h]Controls ≠ PCA, logopenic variant PPA and amnestic Alzheimer's disease; [i]Controls ≠ PCA, logopenic variant PPA; [j]Controls ≠ PCA; [k]Controls < PCA, logopenic variant PPA and amnestic Alzheimer's disease; [l]PCA ≠ logopenic variant PPA.

subjects. In addition, most controls showed tracer uptake in striatum, substantia nigra and choroid plexus thought to represent 'off-target' tracer binding unrelated to tau (Marquie *et al.*, 2015).

^{18}F-AV1451 images of distinct Alzheimer's disease variants

Figure 1 shows a selection of individuals with distinct phenotypes of Alzheimer's disease illustrating the neuroanatomical correspondence between ^{18}F-AV1451 uptake and the clinical presentation. ^{18}F-AV1451 uptake was most prominent in clinically affected posterior regions in PCA (Fig. 1A), the language-dominant left hemisphere in logopenic variant PPA (Fig. 1B) and the basal temporal cortex and medial temporal lobe structures in amnestic-predominant Alzheimer's disease (Fig. 1C). A patient presenting with dysexecutive, visuospatial and language complaints with preserved memory function showed ^{18}F-AV1451 uptake in diffuse parts of the neocortical association cortex with relative sparing of the medial temporal lobes (Fig. 1D). A patient with the behavioural/dysexecutive variant of Alzheimer's disease presenting with impaired organizational skills and judgement, inappropriate behaviour, diminished personal hygiene, hyperorality and newly acquired preference for sweet food, showed ^{18}F-AV1451 uptake in classical temporoparietal regions and—in line with Ossenkoppele *et al.* (2015*c*)—relative sparing of the frontal cortex (Fig. 1E). Finally, a ^{11}C-PiB-positive patient with corticobasal syndrome (mainly affecting the left hemibody) who initially presented with cognitive impairment (i.e. memory and executive dysfunction) showed an asymmetric ^{18}F-AV1451 pattern with greater uptake in the right hemisphere and unique involvement of primary sensorimotor cortex (Fig. 1F), which was spared in other patients.

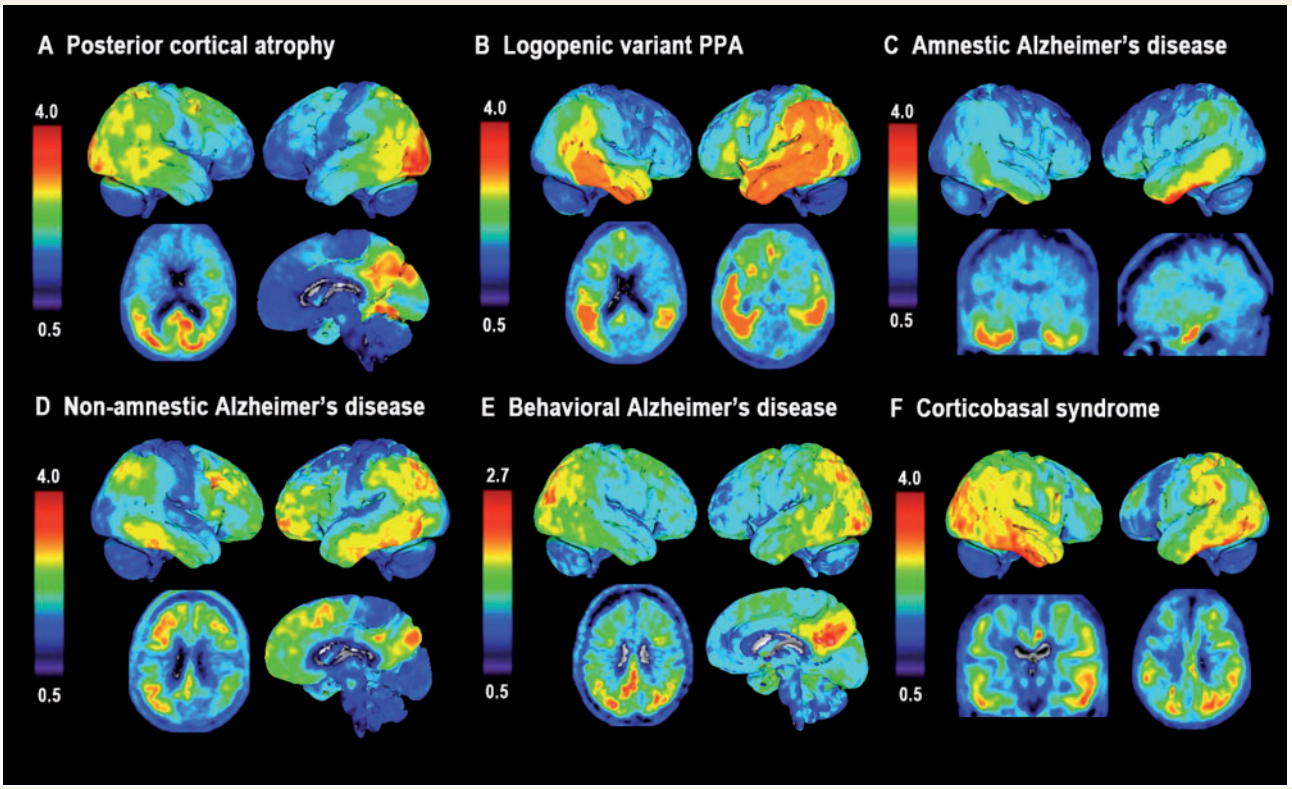

Figure 1 ^{18}F-AV1451 uptake in individuals with distinct phenotypes of Alzheimer's disease. SUVR ^{18}F-AV1451 images (neurological orientation) in (**A**) a 59-year-old female (MMSE: 28) with posterior cortical atrophy [note that this a different patient than presented in Ossenkoppele *et al.* (2015*d*)]; (**B**) a 77-year-old female (MMSE: 17) with logopenic variant PPA; (**C**) a 71-year-old female (MMSE: 23) with amnestic Alzheimer's disease; (**D**) a 59-year-old female (MMSE: 27) with non-amnestic Alzheimer's disease; (**E**) a 59-year-old male (MMSE: 21) with a behavioural presentation of Alzheimer's disease, and (**F**) a 60-year-old female (MMSE: 16) with a corticobasal syndrome affecting the left hemibody.

Voxelwise contrasts between patients and control subjects

Next, we performed voxelwise contrasts for ^{18}F-AV1451, ^{11}C-PiB and ^{18}F-FDG between patients with posterior cortical atrophy and controls. In line with our hypothesis and a previous case study (Ossenkoppele *et al.*, 2015*d*), patients with PCA showed substantial inverse spatial overlap between greater ^{18}F-AV1451 and reduced ^{18}F-FDG uptake, specifically affecting brain regions implicated in higher-order visual processing, particularly in the right hemisphere (Fig. 2A). This is further illustrated by overlaying the binarized ^{18}F-AV1451 and ^{18}F-FDG significance maps (Fig. 2D). Additionally, ^{18}F-AV1451 uptake was elevated in several brain regions where ^{18}F-FDG uptake did not differ from controls, including primary visual cortex and posterior cortex in the left hemisphere. Contrary to the regional specificity of ^{18}F-AV1451 and ^{18}F-FDG, ^{11}C-PiB retention was distributed throughout the neocortex and implicated both clinically affected and relatively spared regions (e.g. extensive binding in frontal cortex; Fig. 2A).

In line with the clinical presentation, the ^{18}F-AV1451 pattern in patients with an amnestic-predominant presentation most prominently affected the medial temporal lobes and lateral temporoparietal cortex (Fig. 2B). When assessing the parametric images and AIs of the five logopenic variant PPA cases individually, three patients showed the predicted left > right asymmetry, one was fairly symmetric, and one showed right > left ^{18}F-AV1451 uptake (Table 2 and Fig. 2E). Notably, the two patients with most advanced disease severity showed the greatest ^{18}F-AV1451 uptake in the right hemisphere and in anterior brain regions. On group-level voxelwise analyses, the ^{18}F-AV1451 pattern in patients with logopenic variant PPA was rather symmetric, with uptake mainly observed in bilateral temporoparietal regions that are typically involved in language function (Fig. 2C). Voxelwise ^{11}C-PiB and ^{18}F-FDG contrasts between amnestic Alzheimer's disease and logopenic variant PPA patients against controls are shown in Supplementary Fig. 3. In general, the results are similar to those seen in patients with PCA (i.e. widespread neocortical ^{11}C-PiB binding, while ^{18}F-FDG uptake is more region-specific), but should be interpreted with caution given the smaller sample size due to missing scans.

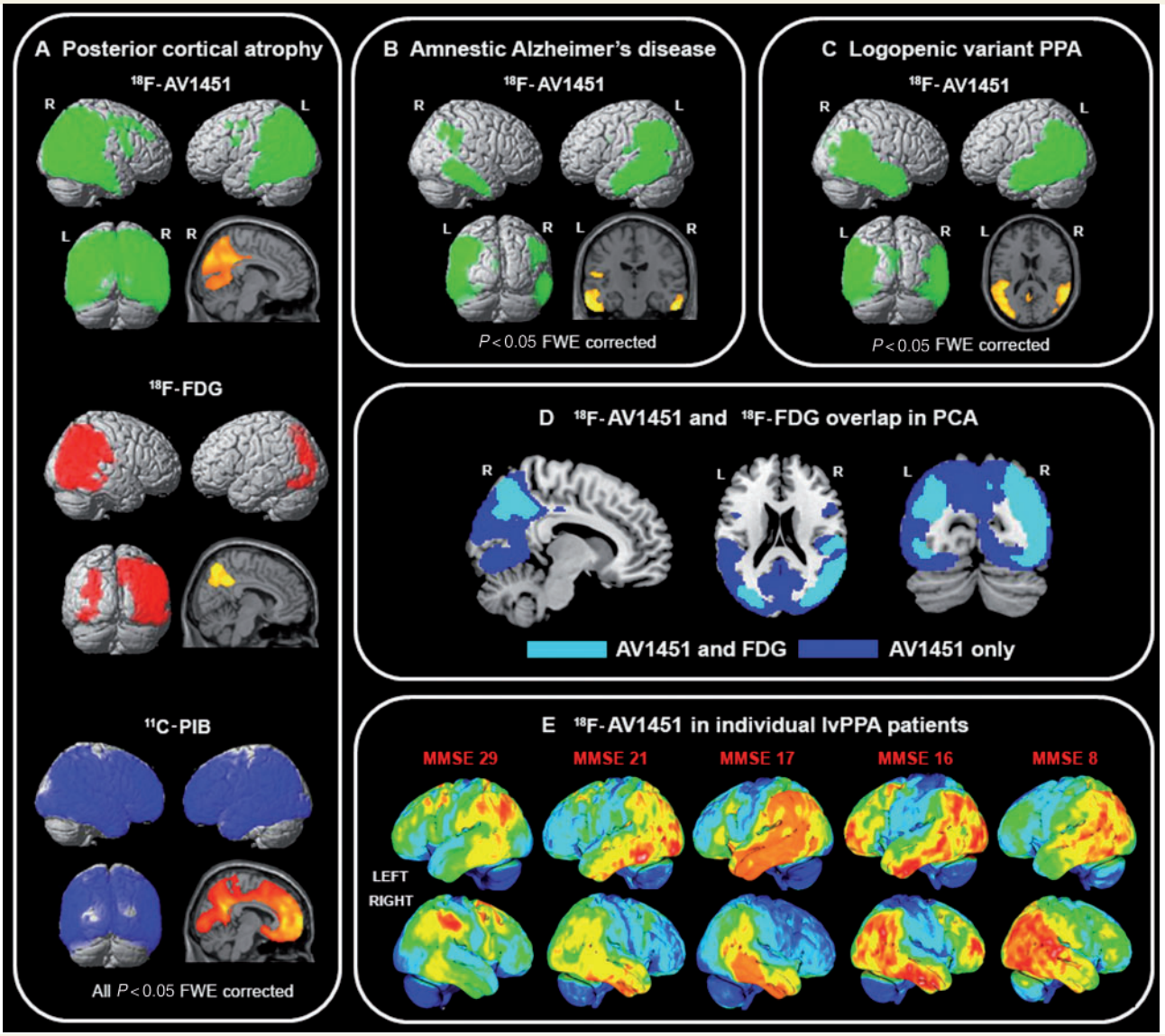

Figure 2 Tracer uptake patterns in patients with different clinical Alzheimer's disease variants. (**A**) Voxelwise contrasts, thresholded at $P < 0.05$ after family-wise error correction and without covariates, indicating regions in which patients with PCA had greater ^{18}F-AV1451 (green), reduced ^{18}F-FDG (red), and elevated ^{11}C-PiB (blue) compared to healthy controls. (**B** and **C**) Contrasts for ^{18}F-AV1451 uptake between amnestic Alzheimer's disease (**B**) and logopenic variant PPA (**C**) patients against healthy controls at $P < 0.05$ after family-wise error correction and without covariates. In panel **D**, we binarized the ^{18}F-AV1451 and ^{18}F-FDG ($P < 0.05$ family-wise error corrected) contrasts between patients with PCA and controls, and show in cyan regions where both ^{18}F-AV1451 and ^{18}F-FDG differed from controls, and in blue brain regions where only the ^{18}F-AV1451 contrast was significant. In **E**, individual ^{18}F-AV1451 images of five logopenic variant PPA patients are displayed in order of their MMSE scores.

Region of interest analyses between ^{18}F-AV1451, ^{11}C-PiB and ^{18}F-FDG PET

Mean uptake values and AIs of ^{18}F-AV1451, ^{11}C-PiB and ^{18}F-FDG in eight regions of interest for each Alzheimer's disease phenotype and the controls are shown in Table 2, Fig. 3, Supplementary Table 2 and Supplementary Fig. 4 (partial volume corrected data).

Bonferroni-corrected ANOVAs showed that patients with PCA had greater ^{18}F-AV1451 retention in occipital and medial parietal (i.e. posterior cingulate and precuneus) regions of interest and reduced ^{18}F-FDG uptake in occipital and lateral parietal regions compared to patients with amnestic and logopenic variant PPA (Table 2 and Fig. 3). Furthermore, patients with amnestic Alzheimer's disease had increased ^{18}F-AV1451 uptake in medial temporal lobe structures compared to the other Alzheimer's disease groups. No differences between the Alzheimer's disease phenotypes were found for ^{11}C-PiB. ^{18}F-AV1451 and ^{18}F-FDG AIs showed R > L asymmetry for PCA, L > R asymmetry for logopenic variant PPA and subtle L > R asymmetry for amnestic

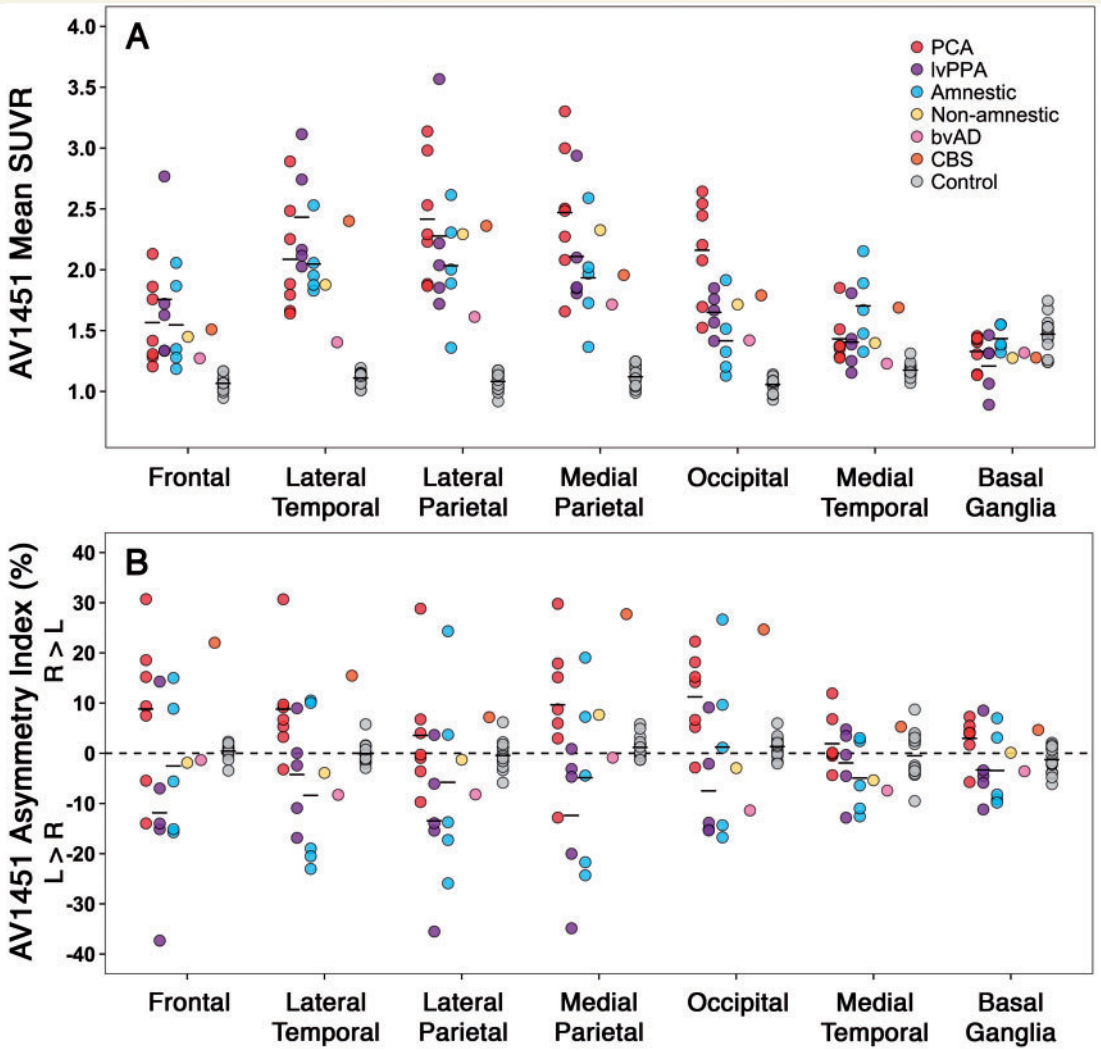

Figure 3 ^{18}F-AV1451 uptake and hemispheric asymmetry in regions of interest. (**A**) ^{18}F-AV1451 SUVR values for each Alzheimer's disease patient and controls in seven bilateral regions of interest. (**B**) The degree of asymmetric tracer uptake within each region of interest as the percentage difference in SUVR value for left compared to right hemisphere: asymmetry index [%] = 200 × (R − L)/(R + L). Table 2 and Supplementary Table 2 show the group means and differences of ^{18}F-AV1451 standardized uptake value ratios and asymmetry indices.

Alzheimer's disease patients across regions of interest (Table 2). No consistent patterns were observed for ^{11}C-PiB. Partial volume correction of the PET data resulted in substantially greater tracer retention values but did not alter any of the differences described above.

Pearson correlation across the different Alzheimer's disease phenotypes ($n = 16$ with all tracers available) in 30 FreeSurfer-defined regions of interest showed a strong association between increased ^{18}F-AV1451 and reduced ^{18}F-FDG uptake (Fig. 4A, Pearson's $r = -0.49 \pm 0.07$, $P < 0.001$). In addition, there were modest positive associations between ^{11}C-PiB DVR and ^{18}F-FDG SUVR (Fig. 4B, Pearson's $r = 0.16 \pm 0.09$, $P < 0.001$) and between ^{18}F-AV1451 SUVR and ^{11}C-PiB DVR (Fig. 4C, Pearson's $r = 0.18 \pm 0.09$, $P < 0.001$). These results were supported by mixed effects models testing relationships between each of the three PET tracers, holding region of interest constant as a fixed effect and subject as a random effect. Mixed effects models showed a significant negative relationship between ^{18}F-AV1451 and ^{18}F-FDG [$\beta = -0.23 \pm 0.01$, $\chi^2(1) = 201.4$, $P < 0.001$], and supported positive associations with smaller effect sizes between ^{11}C-PiB and ^{18}F-FDG [$\beta = 0.29 \pm 0.06$, $\chi^2(1) = 23.5$, $P < 0.001$] and between ^{11}C-PiB and ^{18}F-AV1451 [$\beta = 0.78 \pm 0.15$, $\chi^2(1) = 26.5$, $P < 0.001$]. The relationships between PET tracers in distinct cortical regions (i.e. frontal, parietal, lateral temporal and occipital) are reported in Supplementary Table 3.

Repeating the Pearson correlation analyses using partial volume corrected data, we found a similarly strong association between increased ^{18}F-AV1451 and reduced ^{18}F-FDG uptake (Supplementary Fig. 5A, Pearson's $r = -0.41 \pm 0.07$, $P < 0.001$). In contrast to uncorrected data, the modest positive association between ^{11}C-PiB DVR and

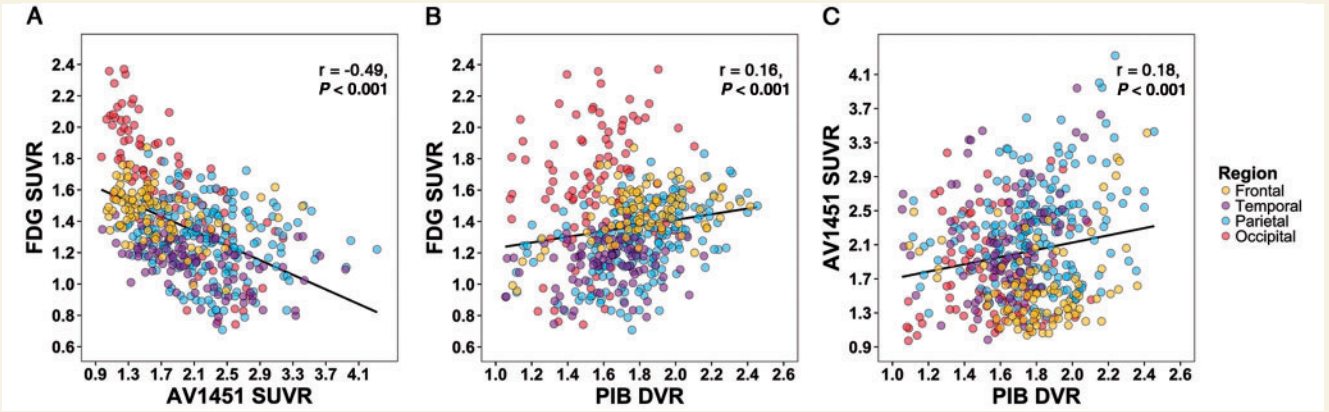

Figure 4 Direct region of interest comparisons between PET tracers. Across 16 Alzheimer's disease patients, regions with greater ^{18}F-AV1451 uptake were strongly associated with lower ^{18}F-FDG metabolism (**A**). Modest, positive associations were also observed between ^{11}C-PiB and ^{18}F-FDG (**B**) and between ^{18}F-AV1451 and ^{11}C-PiB (**C**).

^{18}F-FDG SUVR was no longer significant (Supplementary Fig. 5B, Pearson's r = −0.01 ± 0.09, $P = 0.88$) and the association between ^{18}F-AV1451 SUVR and ^{11}C-PiB DVR was somewhat stronger after applying partial volume correction (Supplementary Fig. 5C, Pearson's r = 0.37 ± 0.08, $P < 0.001$). Mixed effects models of partial volume corrected data showed a significant negative relationship between ^{18}F-AV1451 and ^{18}F-FDG [$\beta = -0.11 \pm 0.01$, $\chi^2(1) = 70.0$, $P < 0.001$], no relationship between ^{11}C-PiB and ^{18}F-FDG [$\beta = 0.02 \pm 0.04$, $\chi^2(1) = 0.2$, $P = 0.642$], and a significant positive relationship between ^{11}C-PiB and ^{18}F-AV1451 [$\beta = 1.52 \pm 0.11$, $\chi^2(1) = 163.8$, $P < 0.001$]. The relationships between partial volume corrected PET tracers in distinct cortical regions (i.e. frontal, parietal, lateral temporal and occipital) are reported in Supplementary Table 3.

Associations of ^{18}F-AV1451 with age and *APOE* ε4 status

Whole-brain voxelwise linear regressions with ^{18}F-AV1451 SUVR and age as continuous variables, thresholded at $P < 0.05$ uncorrected without covariates, showed that younger age was associated with greater ^{18}F-AV1451 uptake in wide regions of the neocortex (Fig. 5A). Several frontal and medial parietal regions survived at $P < 0.01$ uncorrected (Supplementary Fig. 6A). The reverse contrast revealed that older age was associated with increased ^{18}F-AV1451 uptake specifically in the medial temporal lobes (left > right). Consistent with our voxelwise results, region of interest analysis measuring the ratio of hippocampal-to-cortical ^{18}F-AV1451 uptake showed a positive correlation with age [Fig. 5A, $\tau = 0.54$, $P = 0.001$; Supplementary Fig. 7A (partial volume corrected), $\tau = 0.41$, $P = 0.012$].

Voxelwise analysis between *APOE* ε4 status (dichotomous: carriers, non-carriers) and ^{18}F-AV1451 SUVR (continuous), controlling for global amyloid-β burden and thresholded at $P < 0.05$ uncorrected, showed that *APOE* ε4 carriers had greater ^{18}F-AV1451 uptake in bilateral medial temporal and right temporoparietal cortex (Fig. 5B). Supplementary Fig. 6B shows that the right medial temporal lobe survived a slightly more stringent threshold of $P < 0.01$ uncorrected. There were no significant clusters with elevated ^{18}F-AV1451 in *APOE* ε4 non-carriers. The results remained essentially the same when we did not adjust for global amyloid-β burden, and *APOE* ε4 carriers and non-carriers did not differ in age (63.6 ± 9.6 versus 65.2 ± 8.0 years, $P = 0.35$).

Associations of ^{18}F-AV1451 with neuropsychological performance

We performed separate voxelwise linear regressions of MMSE and cognitive domain composite scores on ^{18}F-AV1451 SUVR at a statistical threshold of $P < 0.05$ uncorrected for multiple comparisons and without covariates. Worse MMSE scores were associated with higher ^{18}F-AV1451 uptake in bilateral orbitofrontal cortex (left > right) and left anterior temporal cortex (data not shown). Region of interest analysis showed no relationship between MMSE and whole cortex (i.e. weighted average of frontal, temporal, parietal and occipital cortex) ^{18}F-AV1451 ($\tau = 0.10$, $P = 0.568$, partial volume corrected: $\tau = -0.03$, $P = 0.849$). Patients with lower memory composite scores had higher tracer retention in hippocampus and neighbouring medial temporal regions, with some involvement of inferior temporal cortex (Fig. 6A). Region of interest analyses showed a trend toward worse memory performance with increased ^{18}F-AV1451 uptake in hippocampus (Spearman's *rho* = −0.40, $P = 0.106$; partial volume corrected Spearman's rho = −0.45, $P = 0.063$), while no relationship was observed between memory and whole cortical ^{18}F-AV1451 (Fig. 6A, Spearman's rho = 0.05, $P = 0.844$; partial volume corrected Spearman's rho = −0.19, $P = 0.456$). Worse visuospatial performance correlated with increased ^{18}F-AV1451 in bilateral occipital lobe extending into right temporoparietal regions

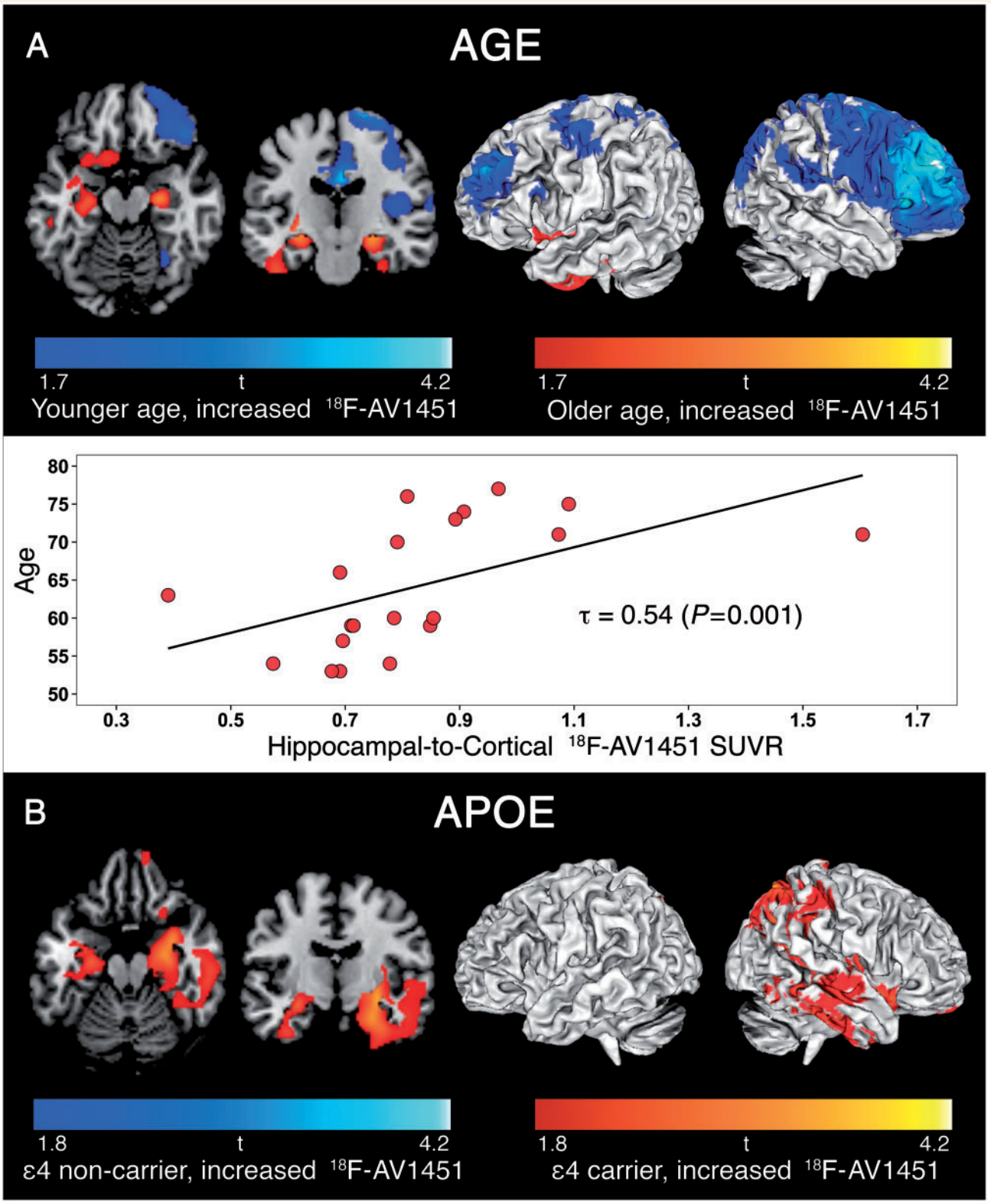

Figure 5 Patterns of ^{18}F-AV1451 retention in Alzheimer's disease associated with age and *APOE* ε4 status. Result from voxelwise linear regression are displayed at $P < 0.05$ uncorrected for multiple comparisons, without covariates for age (**A**), and adjusted for global amyloid-β burden for *APOE* ε4 status (**B**).

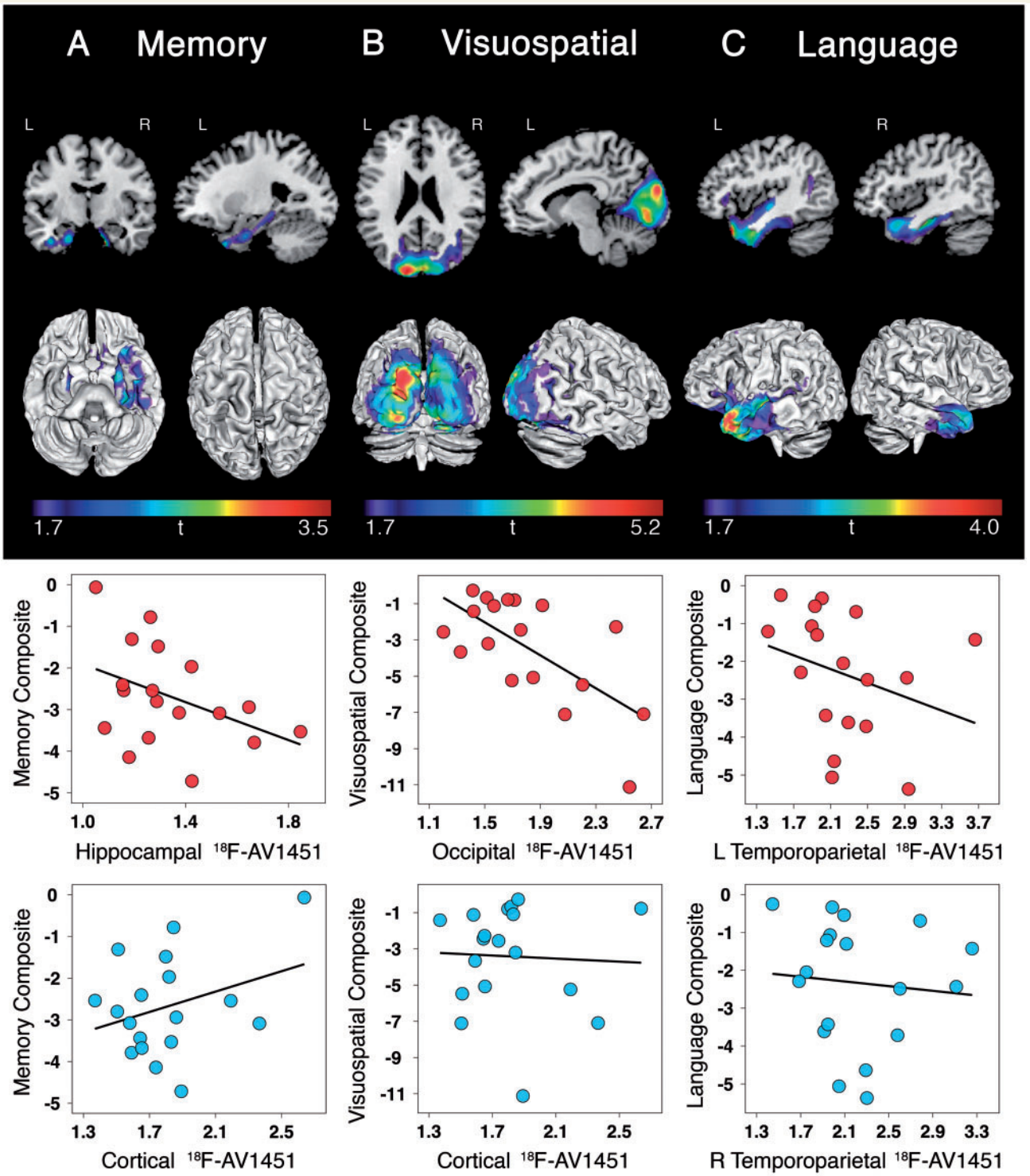

Figure 6 Associations between regional ^{18}F-AV1451 and cognitive performance. Voxelwise contrasts (*top*; $P < 0.05$ uncorrected) show associations between increased ^{18}F-AV1451 retention and worse performance on memory (**A**), visuospatial (**B**), and language testing (**C**). Region of interest analyses (*bottom*) demonstrate that cognitive impairment was associated with focal rather than global increases in ^{18}F-AV1451 in regions underlying specific cognitive domains.

(Fig. 6B). This was confirmed in region of interest analyses showing an association between worse visuospatial performance and elevated ^{18}F-AV1451 in occipital cortex (Spearman's rho = −0.52, $P = 0.028$; partial volume corrected Spearman's rho = −0.51, $P = 0.032$), but not in whole cortex (Fig. 6B, Spearman's rho = 0.11, $P = 0.674$; partial volume corrected Spearman's rho = −0.06, $P = 0.818$). We did not observe a relationship between

worse executive function and greater ^{18}F-AV1451 uptake in any region. Finally, lower language composite scores were associated with elevated ^{18}F-AV1451 uptake in left temporoparietal regions typically implicated in language function, along with smaller clusters in right anterior temporal and inferior frontal cortices (Fig. 6C). In region of interest analyses, worse language performance was correlated with increased ^{18}F-AV1451 uptake in left temporoparietal cortex (Spearman's rho = −0.53, $P = 0.026$; partial volume corrected Spearman's rho = −0.62, $P = 0.007$) but not in right temporoparietal cortex (Spearman's rho = −0.23, $P = 0.366$; partial volume corrected Spearman's rho = −0.37, $P = 0.126$) or whole cortex (Spearman's *rho* = −0.16, $P = 0.53$; partial volume corrected Spearman's rho = −0.33, $P = 0.185$). Supplementary Fig. 6 C–E shows the regions that survived voxelwise linear regression at a more conservative threshold of $P < 0.01$ uncorrected, and Supplementary Fig. 7B–D shows the partial volume corrected region of interest analyses.

Discussion

In this study, we used the novel PET tracer ^{18}F-AV1451 in distinct phenotypes of Alzheimer's disease to examine associations between tau pathology and neuroanatomical and clinical heterogeneity *in vivo*. We found that tau pathology, as measured by ^{18}F-AV1451 PET, preferentially occupied brain areas that are critical for cognitive functions uniquely affected in distinct variants of Alzheimer's disease, and strongly co-localized with hypometabolic regions. In contrast, amyloid-β pathology, as measured by ^{11}C-PiB PET, affected both clinically affected and unaffected regions and showed weak positive (without partial volume correction) or absent (with partial volume correction) associations with regional glucose metabolism. Older age was associated with greater tau pathology in medial temporal lobe structures, while younger patients had greater ^{18}F-AV1451 uptake in the neocortical association cortex. *APOE* ε4 carriers had greater ^{18}F-AV1451 uptake than non-carriers. Finally, increased ^{18}F-AV1451 uptake was associated with worse performance on various cognitive domains in regionally specific patterns, in line with established brain-behaviour relationships. Taken together, these results are consistent with findings from post-mortem, animal and CSF studies, and provide preliminary evidence that the aggregation of tau is closely linked to patterns of neurodegeneration and the clinical manifestations of Alzheimer's disease.

Distinct variants of Alzheimer's disease

In previous studies of typical and atypical clinical presentations of Alzheimer's disease, there has been a dissociation between the rather diffuse distribution of amyloid-β plaques and the highly specific patterns of neurodegeneration that strongly correlate with symptomatology (Rabinovici *et al.*, 2010; Wolk *et al.*, 2012; Lehmann *et al.*, 2013; Jung *et al.*, 2015). It has often been suggested that tau pathology, rather than amyloid-β, may be driving disease manifestation (Desikan *et al.*, 2012; Jack and Holtzman, 2013). Tau imaging with ^{18}F-AV1451 in conjunction with amyloid-β imaging now enables detailed characterization of the two hallmark Alzheimer's disease pathologies *in vivo*. Visual inspection of individual images (Fig. 1) and formal group-level voxelwise analyses (Fig. 2) revealed that tau selectively targeted brain regions that are clinically affected, while amyloid-β was distributed throughout the association cortex (Table 2). For example, ^{18}F-AV1451 was predominantly retained in occipital, parietal and occipitotemporal cortices in patients with PCA, clinically characterized by deficits in primary and higher-order visual processing. Furthermore, patients with an amnestic-predominant presentation showed prominent medial temporal lobe involvement, the patient with a behavioural/dysexecutive presentation had a classical temporoparietal pattern of ^{18}F-AV1451 uptake with relative sparing of the frontal cortex, in line with the atrophy pattern shown in patients with this phenotype (Ossenkoppele *et al.*, 2015c), and the patient with corticobasal syndrome uniquely showed involvement of the peri-rolandic cortex and had greater ^{18}F-AV1451 contralateral to the affected body side. Given the positive ^{11}C-PiB scan, the patient with corticobasal syndrome most likely has Alzheimer's disease, rather than corticobasal degeneration (a 4-repeat tauopathy), as the causal aetiology. Age-related comorbid amyloid-β pathology is unusual at the patient's age (16–18% across cognitively normal persons aged 60; Jack *et al.*, 2014; Jansen *et al.*, 2015) and Alzheimer's disease pathology may be a more frequent cause of corticobasal syndrome in young patients (Ossenkoppele *et al.*, 2015b). Furthermore, glucose hypometabolism was more prominent in temporoparietal than in frontal cortex, which has been associated with underlying Alzheimer's disease pathology in patients with clinical corticobasal syndrome (Sha *et al.*, 2015). Finally, ^{18}F-AV1451 uptake in this patient fell within the Alzheimer's disease range, which is well above the levels we have observed in other patients with suspected corticobasal degeneration (data not shown) and is in line with a recent post-mortem binding study showing that ^{18}F-AV1451 binds to paired helical filaments of tau found in Alzheimer's disease, but not to straight tau filaments found in corticobasal degeneration and other 4-repeat tauopathies (Marquie *et al.*, 2015).

Based on previous neuroimaging studies (Rabinovici *et al.*, 2008; Madhavan *et al.*, 2013; Teichmann *et al.*, 2013; Rogalski *et al.*, 2014; Ossenkoppele *et al.*, 2015*a*) and the specific language presentation, we hypothesized that patients with logopenic variant PPA would show ^{18}F-AV1451 uptake in temporoparietal language regions in a clearly asymmetric fashion with greater tau in the left hemisphere compared to right hemisphere. Visual inspection of individual images and a quantitative laterality index indicated that three logopenic variant PPA showed

the predicted left > right pattern, one was fairly symmetric and one patient had greater ^{18}F-AV1451 uptake in right than in left hemisphere. This is in line with a neuropathological study of primary progressive aphasia due to underlying Alzheimer's disease (Gefen *et al.*, 2012) showing that, while most patients showed higher neurofibrillary pathology in the left hemisphere, a significant minority (14–29% depending on the brain region) had greater tangle pathology in the right hemisphere. At group-level voxelwise analyses, however, the ^{18}F-AV1451 uptake pattern appeared to be fairly symmetrical, largely covering bilateral temporoparietal regions. This finding might be due to the small and heterogeneous sample comprising a wide range of demographic and clinical features. Notably, the two patients with lowest MMSE scores had greater involvement of the right hemisphere and frontal ^{18}F-AV1451 uptake, potentially indicative of tau pathology selectively targeting the left hemisphere in early disease stages and subsequently spreading anteriorly in the left hemisphere and into interconnected contralateral brain regions with advancing disease (Ridgway *et al.*, 2012; Rohrer *et al.*, 2013; Rogalski *et al.*, 2014; Ossenkoppele *et al.*, 2015*a*).

Age and *APOE* ε4

Consistent with previous studies showing selective vulnerability of the medial temporal lobes in late-onset Alzheimer's disease and greater cortical neurodegeneration in early-onset Alzheimer's disease (Rabinovici *et al.*, 2010; Mendez *et al.*, 2012; Smits *et al.*, 2012; Moller *et al.*, 2013; Cavedo *et al.*, 2014), we found that older age was associated with greater ^{18}F-AV1451 uptake in bilateral medial temporal structures, whereas younger age was associated with elevated ^{18}F-AV1451 in occipital, parietal and frontal regions. These different uptake patterns as a function of age highly correspond to the greater overall and neocortical-predominant neurofibrillary tangle burden observed in patients with early-onset Alzheimer's disease at autopsy (Nochlin *et al.*, 1993; Bigio *et al.*, 2002; Marshall *et al.*, 2007). Moreover, we found that *APOE* ε4 carriers had greater ^{18}F-AV1451 uptake in medial and lateral temporal and parietal lobes, even after accounting for global amyloid-β burden. This is consistent with some (Beffert and Poirier, 1996; Tiraboschi *et al.*, 2004) but not all (Schmechel *et al.*, 1993; Greenberg *et al.*, 1995) postmortem studies, and in line with a study showing that *APOE* ε4 directly facilitates phosphorylation of tau resulting in increased filamentous tau load (Harris *et al.*, 2003). Taken together, the present study indicates that factors often linked with heterogeneity in the clinical manifestation of Alzheimer's disease (i.e. age-at-onset and *APOE* ε4 status) are associated with distinct patterns of tau pathology. Our results are also consistent with the neuropathological observation of 'hippocampal-sparing' Alzheimer's disease, where greater tangle burden in cortical versus medial temporal regions is observed in a subset of patients, and is correlated with early age-of-onset, non-amnestic clinical presentations, and lower prevalence of the *APOE* ε4 allele (Murray *et al.*, 2011).

Neuropsychological performance

Expanding upon autopsy and CSF studies describing global associations between tau pathology and cognition (Arriagada *et al.*, 1992; Nelson *et al.*, 2012; van Rossum *et al.*, 2012), we found regionally specific relationships between greater ^{18}F-AV1451 and reduced memory, visuospatial and language functions. In addition, lower MMSE scores were associated with greater ^{18}F-AV1451 uptake in orbitofrontal and anterior temporal cortices. While these may not be considered core Alzheimer's disease regions, they could underscore an anterior spread of tau with advancing disease that coincides with cognitive decline. We did not observe any regional associations between ^{18}F-AV1451 and poor executive function scores, which could be due to difficulty isolating executive function deficits from other cognitive deficits (i.e. visuospatial, language and memory) that may have affected performance on executive function tasks. Similarly, the bilateral ^{18}F-AV1451 pattern associated with worse language performance could be associated with transneuronal spread of tau (Clavaguera *et al.*, 2009; de Calignon *et al.*, 2012; Raj *et al.*, 2012; Zhou *et al.*, 2012) from left hemisphere to right, or with a selective vulnerability of language regions (Rogalski *et al.*, 2008; Miller *et al.*, 2013) to the toxic effects of pathological tau.

Partial volume correction

To assess for confounding effects of atrophy on PET quantification we performed partial volume correction. This yielded substantially higher ^{18}F-AV1451 uptake values in patients, while uptake values remained low by comparison in controls. Additionally, regional asymmetry of ^{18}F-AV1451 uptake was increased after partial volume correction in PCA (right > left) and logopenic variant PPA (left > right) patients but remained equally symmetric in controls. In comparisons between PET tracers in patients, we observed a strong, negative relationship between ^{18}F-AV1451 and ^{18}F-FDG that survived partial volume correction. Furthermore, the association between ^{18}F-AV1451 and ^{11}C-PiB was strengthened after partial volume correction. In contrast, the mildly positive relationship that we initially observed between ^{11}C-PiB and ^{18}F-FDG disappeared after partial volume correction, suggesting this association was largely driven by partial volume effects. Correlations between ^{18}F-AV1451 uptake patterns and neuropsychological performance in patients were similar with and without partial volume correction.

Strengths and limitations

A main strength of the present study is the inclusion of a variety of Alzheimer's disease phenotypes, which allowed

us to study relationships between tau pathology and neuroanatomical and clinical heterogeneity. There are also some limitations. First, this is a preliminary study with a relatively small sample size. Future studies including more patients and a better balance across Alzheimer's disease variants are needed. Second, due to the small sample size, some voxelwise analyses (mainly the associations between tau pathology with age, *APOE* ε4 status and cognition) were conducted at fairly liberal thresholds and should be interpreted with caution, although the relative lack of noise (i.e. focal regional correlations opposed to scattered small clusters) and the convergence of region of interest analyses are encouraging. Third, some patients were missing ^{11}C-PiB and ^{18}F-FDG data (Table 2 and Supplementary Fig. 3), so we could only perform a fair comparison across tracers in patients with PCA (Fig. 2). Fourth, we did not assess relationships between molecular markers and brain atrophy because T_1-weighted MRI was acquired at different scanners for patients and controls. Finally, as the healthy controls were significantly older than our relatively young Alzheimer's disease patients, we did not adjust our voxelwise contrasts (Fig. 2) to avoid collinearity between age and ^{18}F-AV1451 uptake.

Future directions

Tau imaging will help address fundamental questions about the mechanisms that drive clinical, anatomical and functional diversity in Alzheimer's disease. Key topics for future research include the further study of cross-sectional and longitudinal relationships between tau, amyloid-β and neurodegeneration, and how each of these factors contributes to clinical progression. Understanding which protein is the major force driving neurodegeneration and cognitive decline is highly relevant for developing and testing effective therapies, and the advent of novel tau PET tracers (Villemagne *et al.*, 2015) will for the first time allow in-depth testing of the entire amyloid cascade hypothesis (Hardy, 2009) *in vivo*.

Acknowledgements

We would like to thank Kristin Norton, Jamie Faria, Vyoma Shah, and Allison Fero for their contributions in the acquisition and analysis of PET data, and Giovanni Coppola and Anna Karydas for *APOE* genotyping.

Funding

This research was funded by Marie Curie FP7 International Outgoing Fellowship (628812; to R.O.); The donors of (Alzheimer's Disease Research), a program of BrightFocus Foundation (to R.O.); Tau Consortium (to G.D.R. and W.J.J); National Institute on Aging grants (R01-AG045611; to G.D.R.), (R01-AG034570; to W.J.J.), (P50-AG023501; to B.L.M.), and (K23-AG038357; to K.A.V.); John Douglas French Alzheimer's Foundation (to G.D.R. and B.L.M.); State of California Department of Health Services Alzheimer's Disease Research Centre of California grant (04-33516; to B.L.M); Swedish Medical Association and the Swedish Foundation of Nuclear Medicine (to M.S.). Avid Radiopharmaceuticals enabled use of the ^{18}F-AV1451 tracer, but did not provide direct funding and was not involved in data analysis or interpretation.

Supplementary material

Supplementary material is available at *Brain* online.

References

Albert MS, DeKosky ST, Dickson D, Dubois B, Feldman HH, Fox NC, et al. The diagnosis of mild cognitive impairment due to Alzheimer's disease: recommendations from the National Institute on Aging-Alzheimer's Association workgroups on diagnostic guidelines for Alzheimer's disease. Alzheimers Dement 2011; 7: 270–9.

Armstrong MJ. Diagnosis and treatment of corticobasal degeneration. Curr Treat Options Neurol 2014; 16: 282.

Arriagada PV, Growdon JH, Hedley-Whyte ET, Hyman BT. Neurofibrillary tangles but not senile plaques parallel duration and severity of Alzheimer's disease. Neurology 1992; 42: 631–9.

Barthel H, Gertz HJ, Dresel S, Peters O, Bartenstein P, Buerger K, et al. Cerebral amyloid-beta PET with florbetaben (18F) in patients with Alzheimer's disease and healthy controls: a multicentre phase 2 diagnostic study. Lancet Neurol 2011; 10: 424–35.

Beffert U, Poirier J. Apolipoprotein E, plaques, tangles and cholinergic dysfunction in Alzheimer's disease. Ann N Y Acad Sci 1996; 777: 166–74.

Beharry C, Cohen LS, Di J, Ibrahim K, Briffa-Mirabella S, Alonso Adel C. Tau-induced neurodegeneration: mechanisms and targets. Neurosci Bull 2014; 30: 346–58.

Bigio EH, Hynan LS, Sontag E, Satumtira S, White CL. Synapse loss is greater in presenile than senile onset Alzheimer disease: implications for the cognitive reserve hypothesis. Neuropathol Appl Neurobiol 2002; 28: 218–27.

Braak H, Braak E. Neuropathological stageing of Alzheimer-related changes. Acta Neuropathol 1991; 82: 239–59.

Cavedo E, Pievani M, Boccardi M, Galluzzi S, Bocchetta M, Bonetti M, et al. Medial temporal atrophy in early and late-onset Alzheimer's disease. Neurobiol Aging 2014; 35: 2004–12.

Chien DT, Bahri S, Szardenings AK, Walsh JC, Mu F, Su MY, et al. Early clinical PET imaging results with the novel PHF-tau radioligand [F-18]-T807. J Alzheimer Dis 2013; 34: 457–68.

Clark CM, Schneider JA, Bedell BJ, Beach TG, Bilker WB, Mintun MA, et al. Use of florbetapir-PET for imaging beta-amyloid pathology. JAMA 2011; 305: 275–83.

Clavaguera F, Bolmont T, Crowther RA, Abramowski D, Frank S, Probst A, et al. Transmission and spreading of tauopathy in transgenic mouse brain. Nat Cell Biol 2009; 11: 909–13.

Coppola G, Chinnathambi S, Lee JJ, Dombroski BA, Baker MC, Soto-Ortolaza AI, et al. Evidence for a role of the rare p.A152T variant in MAPT in increasing the risk for FTD-spectrum and Alzheimer's diseases. Hum Mol Genet 2012; 21: 3500–12.

Crutch SJ, Lehmann M, Schott JM, Rabinovici GD, Rossor MN, Fox NC. Posterior cortical atrophy. Lancet Neurol 2012; 11: 170–8.

de Calignon A, Polydoro M, Suarez-Calvet M, William C, Adamowicz DH, Kopeikina KJ, et al. Propagation of tau pathology in a model of early Alzheimer's disease. Neuron 2012; 73: 685–97.

Desikan RS, McEvoy LK, Thompson WK, Holland D, Brewer JB, Aisen PS, et al. Amyloid-beta–associated clinical decline occurs only in the presence of elevated P-tau. Arch Neurol 2012; 69: 709–13.

Dickson DW, Bergeron C, Chin SS, Duyckaerts C, Horoupian D, Ikeda K, et al. Office of rare diseases neuropathologic criteria for corticobasal degeneration. J Neuropathol Exp Neurol 2002; 61: 935–46.

Dubois B, Feldman HH, Jacova C, Hampel H, Molinuevo JL, Blennow K, et al. Advancing research diagnostic criteria for Alzheimer's disease: the IWG-2 criteria. Lancet Neurol 2014; 13: 614–29.

Fischl B, Salat DH, Busa E, Albert M, Dieterich M, Haselgrove C, et al. Whole brain segmentation: automated labeling of neuroanatomical structures in the human brain. Neuron 2002; 33: 341–55.

Frings L, Hellwig S, Spehl TS, Bormann T, Buchert R, Vach W, et al. Asymmetries of amyloid-beta burden and neuronal dysfunction are positively correlated in Alzheimer's disease. Brain 2015; 138: 3089–99.

Gefen T, Gasho K, Rademaker A, Lalehzari M, Weintraub S, Rogalski E, et al. Clinically concordant variations of Alzheimer pathology in aphasic versus amnestic dementia. Brain 2012; 135: 1554–65.

Gomez-Isla T, Hollister R, West H, Mui S, Growdon JH, Petersen RC, et al. Neuronal loss correlates with but exceeds neurofibrillary tangles in Alzheimer's disease. Ann Neurol 1997; 41: 17–24.

Gorno-Tempini ML, Hillis AE, Weintraub S, Kertesz A, Mendez M, Cappa SF, et al. Classification of primary progressive aphasia and its variants. Neurology 2011; 76: 1006–14.

Greenberg SM, Rebeck GW, Vonsattel JP, Gomez-Isla T, Hyman BT. Apolipoprotein E epsilon 4 and cerebral hemorrhage associated with amyloid angiopathy. Ann Neurol 1995; 38: 254–9.

Grundman M, Pontecorvo MJ, Salloway SP, Doraiswamy PM, Fleisher AS, Sadowsky CH, et al. Potential impact of amyloid imaging on diagnosis and intended management in patients with progressive cognitive decline. Alzheimer Dis Assoc Disord 2013; 27: 4–15.

Hardy J. The amyloid hypothesis for Alzheimer's disease: a critical reappraisal. J Neurochem 2009; 110: 1129–34.

Harris FM, Brecht WJ, Xu Q, Tesseur I, Kekonius L, Wyss-Coray T, et al. Carboxyl-terminal-truncated apolipoprotein E4 causes Alzheimer's disease-like neurodegeneration and behavioral deficits in transgenic mice. Proc Nat Acad Sci USA 2003; 100: 10966–71.

Jack CR Jr, Holtzman DM. Biomarker modeling of Alzheimer's disease. Neuron 2013; 80: 1347–58.

Jack CR Jr, Wiste HJ, Weigand SD, Rocca WA, Knopman DS, Mielke MM, et al. Age-specific population frequencies of cerebral beta-amyloidosis and neurodegeneration among people with normal cognitive function aged 50-89 years: a cross-sectional study. Lancet Neurol 2014; 13: 997–1005.

Jansen WJ, Ossenkoppele R, Knol DL, Tijms BM, Scheltens P, Verhey FR, et al. Prevalence of cerebral amyloid pathology in persons without dementia: a meta-analysis. JAMA 2015; 313: 1924–38.

Johnson KA, Schultz A, Betensky RA, Becker JA, Sepulcre J, Rentz D, et al. Tau PET imaging in aging and early Alzheimer's disease. Ann Neurol 2016; 79: 110–19.

Jung Y, Whitwell JL, Duffy JR, Strand EA, Machulda MM, Senjem ML, et al. Regional beta-amyloid burden does not correlate with cognitive or language deficits in Alzheimer's disease presenting as aphasia. Eur J Neurol 2016; 23: 313–9.

Klunk WE, Engler H, Nordberg A, Wang Y, Blomqvist G, Holt DP, et al. Imaging brain amyloid in Alzheimer's disease with Pittsburgh Compound-B. Ann Neurol 2004; 55: 306–19.

Kramer JH, Jurik J, Sha SJ, Rankin KP, Rosen HJ, Johnson JK, et al. Distinctive neuropsychological patterns in frontotemporal dementia, semantic dementia, and Alzheimer disease. Cogn Behav Neurol 2003; 16: 211–18.

Lee SE, Rabinovici GD, Mayo MC, Wilson SM, Seeley WW, DeArmond SJ, et al. Clinicopathological correlations in corticobasal degeneration. Ann Neurol 2011; 70: 327–40.

Lehmann M, Ghosh PM, Madison C, Karydas A, Coppola G, O'Neil JP, et al. Greater medial temporal hypometabolism and lower cortical amyloid burden in ApoE4-positive AD patients. J Neurol Neurosurg Psychiatry 2014; 85: 266–73.

Lehmann M, Ghosh PM, Madison C, Laforce R Jr, Corbetta-Rastelli C, Weiner MW, et al. Diverging patterns of amyloid deposition and hypometabolism in clinical variants of probable Alzheimer's disease. Brain 2013; 136: 844–58.

Liu E, Schmidt ME, Margolin R, Sperling R, Koeppe R, Mason NS, et al. Amyloid-beta 11C-PiB-PET imaging results from 2 randomized bapineuzumab phase 3 AD trials. Neurology 2015; 85: 692–700.

Logan J, Fowler JS, Volkow ND, Wang GJ, Ding YS, Alexoff DL. Distribution volume ratios without blood sampling from graphical analysis of PET data. J Cereb Blood Flow Metab 1996; 16: 834–40.

Madhavan A, Whitwell JL, Weigand SD, Duffy JR, Strand EA, Machulda MM, et al. FDG PET and MRI in logopenic primary progressive aphasia versus dementia of the Alzheimer's type. PloS One 2013; 8: e62471.

Marshall GA, Fairbanks LA, Tekin S, Vinters HV, Cummings JL. Early-onset Alzheimer's disease is associated with greater pathologic burden. J Geriatr Psychiatry Neurol 2007; 20: 29–33.

Marquie M, Normandin MD, Vanderburg CR, Costantino I, Bien EA, Rycyna LG, et al. Validating novel tau PET tracer [F-18]-AV-1451 (T807) on postmortem brain tissue. Ann Neurol 2015; 78: 787–800.

McKhann GM, Knopman DS, Chertkow H, Hyman BT, Jack CR Jr, Kawas CH, et al. The diagnosis of dementia due to Alzheimer's disease: recommendations from the National Institute on Aging-Alzheimer's Association workgroups on diagnostic guidelines for Alzheimer's disease. Alzheimers 2011; 7: 263–9.

Mendez MF, Ghajarania M, Perryman KM. Posterior cortical atrophy: clinical characteristics and differences compared to Alzheimer's disease. Dement Geriatr Cogn Disord 2002; 14: 33–40.

Mendez MF, Lee AS, Joshi A, Shapira JS. Nonamnestic presentations of early-onset Alzheimer's disease. Am J Alzheimer Dis Other Dement 2012; 27: 413–20.

Miller ZA, Mandelli ML, Rankin KP, Henry ML, Babiak MC, Frazier DT, et al. Handedness and language learning disability differentially distribute in progressive aphasia variants. Brain 2013; 136: 3461–73.

Minoshima S, Frey KA, Foster NL, Kuhl DE. Preserved pontine glucose metabolism in Alzheimer disease: a reference region for functional brain image (PET) analysis. J Compu Assist Tomography 1995; 19: 541–7.

Moller C, Vrenken H, Jiskoot L, Versteeg A, Barkhof F, Scheltens P, et al. Different patterns of gray matter atrophy in early- and late-onset Alzheimer's disease. Neurobiol Aging 2013; 34: 2014–22.

Mormino EC, Brandel MG, Madison CM, Rabinovici GD, Marks S, Baker SL, et al. Not quite PIB-positive, not quite PIB-negative: slight PIB elevations in elderly normal control subjects are biologically relevant. NeuroImage 2012; 59: 1152–60.

Murray ME, Graff-Radford NR, Ross OA, Petersen RC, Duara R, Dickson DW. Neuropathologically defined subtypes of Alzheimer's disease with distinct clinical characteristics: a retrospective study. Lancet Neurol 2011; 10: 785–96.

Nelson PT, Alafuzoff I, Bigio EH, Bouras C, Braak H, Cairns NJ, et al. Correlation of Alzheimer disease neuropathologic changes with cognitive status: a review of the literature. J Neuropathol Exp Neurol 2012; 71: 362–81.

Nochlin D, van Belle G, Bird TD, Sumi SM. Comparison of the severity of neuropathologic changes in familial and sporadic Alzheimer's disease. Alzheimer Dis Assoc Disord 1993; 7: 212–22.

Ossenkoppele R, Cohn-Sheehy BI, La Joie R, Vogel JW, Moller C, Lehmann M, et al. Atrophy patterns in early clinical stages across

distinct phenotypes of Alzheimer's disease. Hum Brain Mapp 2015a; 36: 4421–37.

Ossenkoppele R, Jansen WJ, Rabinovici GD, Knol DL, van der Flier WM, van Berckel BN, et al. Prevalence of amyloid PET positivity in dementia syndromes: a meta-analysis. JAMA 2015b; 313: 1939–49.

Ossenkoppele R, Madison C, Oh H, Wirth M, van Berckel BN, Jagust WJ. Is verbal episodic memory in elderly with amyloid deposits preserved through altered neuronal function? Cerebral Cortex 2014; 24: 2210–18.

Ossenkoppele R, Pijnenburg YA, Perry DC, Cohn-Sheehy BI, Scheltens NM, Vogel JW, et al. The behavioural/dysexecutive variant of Alzheimer's disease: clinical, neuroimaging and pathological features. Brain 2015c; 138: 2732–49.

Ossenkoppele R, Prins ND, Pijnenburg YA, Lemstra AW, van der Flier WM, Adriaanse SF, et al. Impact of molecular imaging on the diagnostic process in a memory clinic. Alzheimers Dement 2013a; 9: 414–21.

Ossenkoppele R, Schonhaut DR, Baker SL, O'Neil JP, Janabi M, Ghosh PM, et al. Tau, amyloid, and hypometabolism in a patient with posterior cortical atrophy. Ann Neurol 2015d; 77: 338–42.

Ossenkoppele R, van der Flier WM, Zwan MD, Adriaanse SF, Boellaard R, Windhorst AD, et al. Differential effect of APOE genotype on amyloid load and glucose metabolism in AD dementia. Neurology 2013b; 80: 359–65.

Ossenkoppele R, Zwan MD, Tolboom N, van Assema DM, Adriaanse SF, Kloet RW, et al. Amyloid burden and metabolic function in early-onset Alzheimer's disease: parietal lobe involvement. Brain 2012; 135: 2115–25.

Pievani M, Rasser PE, Galluzzi S, Benussi L, Ghidoni R, Sabattoli F, et al. Mapping the effect of APOE epsilon4 on gray matter loss in Alzheimer's disease in vivo. NeuroImage 2009; 45: 1090–8.

Rabinovici GD, Furst AJ, Alkalay A, Racine CA, O'Neil JP, Janabi M, et al. Increased metabolic vulnerability in early-onset Alzheimer's disease is not related to amyloid burden. Brain 2010; 133: 512–28.

Rabinovici GD, Jagust WJ, Furst AJ, Ogar JM, Racine CA, Mormino EC, et al. Abeta amyloid and glucose metabolism in three variants of primary progressive aphasia. Ann Neurol 2008; 64: 388–401.

Raj A, Kuceyeski A, Weiner M. A network diffusion model of disease progression in dementia. Neuron 2012; 73: 1204–15.

Ridgway GR, Lehmann M, Barnes J, Rohrer JD, Warren JD, Crutch SJ, et al. Early-onset Alzheimer disease clinical variants: multivariate analyses of cortical thickness. Neurology 2012; 79: 80–4.

Rogalski E, Cobia D, Martersteck A, Rademaker A, Wieneke C, Weintraub S, et al. Asymmetry of cortical decline in subtypes of primary progressive aphasia. Neurology 2014; 83: 1184–91.

Rogalski E, Johnson N, Weintraub S, Mesulam M. Increased frequency of learning disability in patients with primary progressive aphasia and their first-degree relatives. Arch Neurol 2008; 65: 244–8.

Rohrer JD, Caso F, Mahoney C, Henry M, Rosen HJ, Rabinovici G, et al. Patterns of longitudinal brain atrophy in the logopenic variant of primary progressive aphasia. Brain Lang 2013; 127: 121–6.

Rolstad S, Berg AI, Bjerke M, Johansson B, Zetterberg H, Wallin A. Cerebrospinal fluid biomarkers mirror rate of cognitive decline. J Alzheimers Dis 2013; 34: 949–56.

Rousset OG, Ma Y, Evans AC. Correction for partial volume effects in PET: principle and validation. J Nucl Med 1998; 39: 904–11.

Salloway S, Sperling R, Fox NC, Blennow K, Klunk W, Raskind M, et al. Two phase 3 trials of bapineuzumab in mild-to-moderate Alzheimer's disease. New Engl J Med 2014; 370: 322–33.

Sanchez-Juan P, Ghosh PM, Hagen J, Gesierich B, Henry M, Grinberg LT, et al. Practical utility of amyloid and FDG-PET in an academic dementia center. Neurology 2014; 82: 230–8.

Schipke CG, Peters O, Heuser I, Grimmer T, Sabbagh MN, Sabri O, et al. Impact of beta-amyloid-specific florbetaben PET imaging on confidence in early diagnosis of Alzheimer's disease. Dement Geriatr Cogn Disord 2012; 33: 416–22.

Schmechel DE, Saunders AM, Strittmatter WJ, Crain BJ, Hulette CM, Joo SH, et al. Increased amyloid beta-peptide deposition in cerebral cortex as a consequence of apolipoprotein E genotype in late-onset Alzheimer disease. Proc Nat Acad Sci USA 1993; 90: 9649–53.

Sha SJ, Ghosh PM, Lee SE, Corbetta-Rastelli C, Jagust WJ, Kornak J, et al. Predicting amyloid status in corticobasal syndrome using modified clinical criteria, magnetic resonance imaging and fluorodeoxyglucose positron emission tomography. Alzheimers Res Ther 2015; 7: 8.

Smits LL, Pijnenburg YA, Koedam EL, van der Vlies AE, Reuling IE, Koene T, et al. Early onset Alzheimer's disease is associated with a distinct neuropsychological profile. J Alzheimers Dis 2012; 30: 101–8.

Sperling RA, Aisen PS, Beckett LA, Bennett DA, Craft S, Fagan AM, et al. Toward defining the preclinical stages of Alzheimer's disease: recommendations from the National Institute on Aging-Alzheimer's Association workgroups on diagnostic guidelines for Alzheimer's disease. Alzheimers Dement 2011; 7: 280–92.

Spires-Jones TL, Hyman BT. The intersection of amyloid beta and tau at synapses in Alzheimer's disease. Neuron 2014; 82: 756–71.

Teichmann M, Kas A, Boutet C, Ferrieux S, Nogues M, Samri D, et al. Deciphering logopenic primary progressive aphasia: a clinical, imaging and biomarker investigation. Brain 2013; 136: 3474–88.

Tiraboschi P, Hansen LA, Masliah E, Alford M, Thal LJ, Corey-Bloom J. Impact of APOE genotype on neuropathologic and neurochemical markers of Alzheimer disease. Neurology 2004; 62: 1977–83.

van der Flier WM, Pijnenburg YA, Fox NC, Scheltens P. Early-onset versus late-onset Alzheimer's disease: the case of the missing APOE epsilon4 allele. Lancet Neurol 2011; 10: 280–8.

van Rossum IA, Visser PJ, Knol DL, van der Flier WM, Teunissen CE, Barkhof F, et al. Injury markers but not amyloid markers are associated with rapid progression from mild cognitive impairment to dementia in Alzheimer's disease. J Alzheimers Dis 2012; 29: 319–27.

Vandenberghe R, Van Laere K, Ivanoiu A, Salmon E, Bastin C, Triau E, et al. 18F-flutemetamol amyloid imaging in Alzheimer disease and mild cognitive impairment: a phase 2 trial. Ann Neurol 2010; 68: 319–29.

Villemagne VL, Fodero-Tavoletti MT, Masters CL, Rowe CC. Tau imaging: early progress and future directions. Lancet Neurol 2015; 14: 114–24.

Villeneuve S, Reed BR, Madison CM, Wirth M, Marchant NL, Kriger S, et al. Vascular risk and Abeta interact to reduce cortical thickness in AD vulnerable brain regions. Neurology 2014; 83: 40–7.

Weingarten MD, Lockwood AH, Hwo SY, Kirschner MW. A protein factor essential for microtubule assembly. Proc Nat Acad Sci USA 1975; 72: 1858–62.

Wolk DA, Price JC, Madeira C, Saxton JA, Snitz BE, Lopez OL, et al. Amyloid imaging in dementias with atypical presentation. Alzheimers Dement 2012; 8: 389–98.

Xia CF, Arteaga J, Chen G, Gangadharmath U, Gomez LF, Kasi D, et al. [(18)F]T807, a novel tau positron emission tomography imaging agent for Alzheimer's disease. Alzheimers Dement 2013; 9: 666–76.

Zhou J, Gennatas ED, Kramer JH, Miller BL, Seeley WW. Predicting regional neurodegeneration from the healthy brain functional connectome. Neuron 2012; 73: 1216–27.